NASA
Technical
Memorandum

NASA TM-86516

SURFACE VOLTAGE GRADIENT ROLE IN HIGH VOLTAGE SOLAR ARRAY/PLASMA INTERACTIONS

Center Director's Discretionary Fund Final Report

By M. R. Carruth, Jr

Space Science Laboratory

July 1985

National Aeronautics and
Space Administration

George C. Marshall Space Flight Center

TECHNICAL REPORT STANDARD TITLE PAGE

1. REPORT NO.	2. GOVERNMENT ACCESSION NO.	3. RECIPIENT'S CATALOG NO.
NASA TM-86516		

4. TITLE AND SUBTITLE	5. REPORT DATE
Surface Voltage Gradient Role in High Voltage Solar Array/Plasma Interactions — Center Director's Discretionary Fund Final Report	July 1985
	6. PERFORMING ORGANIZATION CODE
7. AUTHOR(S)	8. PERFORMING ORGANIZATION REPORT #
M. R. Carruth, Jr.	
9. PERFORMING ORGANIZATION NAME AND ADDRESS	10. WORK UNIT NO.
George C. Marshall Space Flight Center Marshall Space Flight Center, Alabama 35812	11. CONTRACT OR GRANT NO.
	13. TYPE OF REPORT & PERIOD COVERED
12. SPONSORING AGENCY NAME AND ADDRESS	Technical Memorandum
National Aeronautics and Space Administration Washington, D.C. 20546	14. SPONSORING AGENCY CODE

15. SUPPLEMENTARY NOTES

Prepared by Space Science Laboratory, Science and Engineering Directorate.

16. ABSTRACT

A large amount of experimental and analytical effort has been directed toward understanding the plasma sheath growth and discharge phenomena which lead to high voltage solar array-space plasma interactions. An important question which has not been addressed is how the surface voltage gradient on such an array may affect these interactions. The results of this study indicate that under certain conditions, the voltage gradient should be taken into account when evaluating the effect on a solar array operating in a plasma environment.

17. KEY WORDS	18. DISTRIBUTION STATEMENT
Solar Array Plasma Interactions Spacecraft Charging	Unclassified — Unlimited

19. SECURITY CLASSIF. (of this report)	20. SECURITY CLASSIF. (of this page)	21. NO. OF PAGES	22. PRICE
Unclassified	Unclassified	40	NTIS

MSFC - Form 3292 (May 1969)

For sale by National Technical Information Service, Springfield, Virginia 22151

TABLE OF CONTENTS

LIST OF ILLUSTRATIONS

LIST OF ILLUSTRATIONS (Concluded)

NOMENCLATURE

A_p	area of Langmuir probe surface
a	effective hole radius or slit half-width
d	slit separation; center to center
E	electric field
e	electron unit charge
m_e	electron mass
n_e	electron density
r	radial component of cylindrical coordinate system
s	slope of current squared versus voltage for accelerating region of cylindrical Langmuir probe characteristic
x	coordinate perpendicular to slit axis and Z; cartesian coordinate system
z	coordinate axis perpendicular to plane of test article
T_e	electron temperature
V_p	Langmuir probe potential relative to plasma potential
α	characteristic length for potential change on Z axis
λ	characteristic length for potential change on r or x coordinate
ϕ	electric potential

TECHNICAL MEMORANDUM

SURFACE VOLTAGE GRADIENT ROLE IN HIGH VOLTAGE SOLAR ARRAY/PLASMA INTERACTIONS

Center Director's Discretionary Fund Final Report

INTRODUCTION

Most U.S. spacecraft have used low voltage solar arrays, generating power near 30 V. The highest voltage array flown by NASA was on Skylab, which had a solar array with a normal operating voltage of 70 V and generated 16 kW of power. Future large systems will require increasing power generation capability. For example, a solar array providing energy for a low inclination, low altitude 50 kW space system will need to generate about 100 kW of power when in sunlight. As power levels increase, the mass, I^2R power loss, and power distribution system complexity penalties for maintaining low solar array voltages become prohibitive, making higher voltage array designs mandatory [1]. Thus, it is necessary to thoroughly understand high voltage solar array operation in the space plasma environment.

Solar array systems consist of strings of solar cells with metallic interconnects between them. These interconnects are at voltages depending upon their positions in the array circuit and are usually exposed to the space environment. When such systems are placed in orbit, they will interact with the naturally occurring space plasma. Two types of potentially hazardous interactions to a higher voltage solar array in orbit are presently recognized: power loss from parasitic currents through the plasma and arcing on the array. Both of these interactions are plasma density dependent and present greater hazards at higher densities. The low temperature ionospheric plasma has a peak density on the order of 10^6 particles/cm^3 at about 300 km altitude. High voltage system-plasma interactions will therefore be most severe in low Earth orbits. The power levels envisioned for future, large spacecraft drive the design toward higher solar array operating voltages. When the spacecraft exits eclipse, this voltage will be even higher until the array warms to normal operating temperature. Successful design of higher voltage arrays relies on understanding the limits imposed by plasma interactions.

A spacecraft in orbit and immersed in the space plasma will come to a potential relative to the plasma such that no net current is collected by the spacecraft as a whole. The solar array provides an additional complication, however, since ambient charge particles can be collected by it. There are two solar array voltages to consider. One is the operating voltage generated by the solar cells in series. The other is the potential of the solar array relative to the surrounding space plasma. Some point on the array will be at space potential and the portions of the solar array positive of this point will collect electrons from the plasma while the negative part collects ions or emits electrons. Therefore, to collect equal electron and ion current, a much larger area at a negative potential relative to the plasma is required. For a spacecraft grounded to the negative side of the solar array, the situation on the right side of Figure 1 will result. The spacecraft and negative side of the array will be driven below space potential. For an array of several hundred volts, solar array

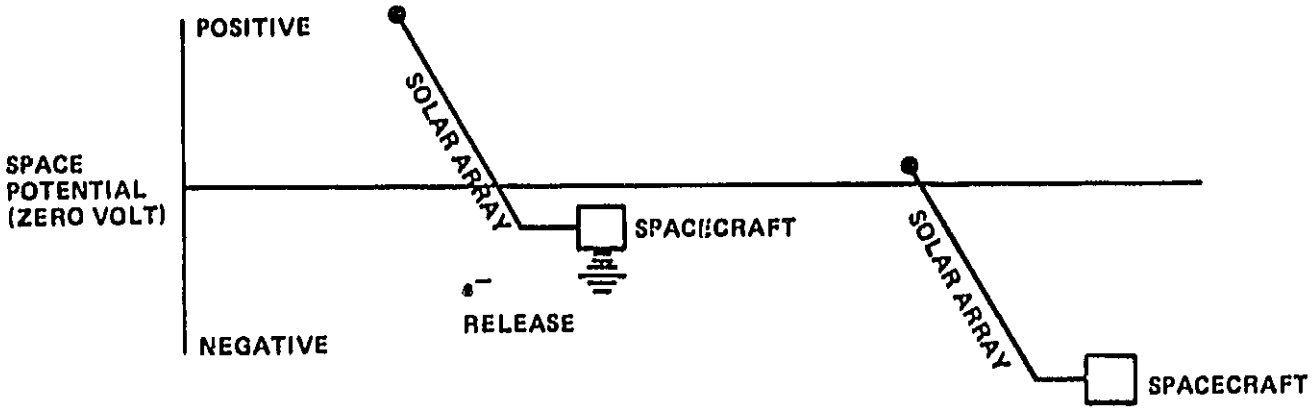

Figure 1. Solar array-spacecraft-ambient space relative potentials.

arcing may result, and since the spacecraft structure will be several hundred volts negative, it will experience a continuous ion bombardment for the spacecraft lifetime which may alter surface thermo-optical properties. Another spacecraft without such a solar array or an untethered astronaut will be near space potential. The resulting potential difference between such a free flyer and a highly negative spacecraft can pose serious safety concerns. The highly negative spacecraft potential will also interfere with some science, e.g., particle and plasma data acquisition.

If an electron gun or plasma source is operated on the spacecraft, electrons collected by the positive portion of the solar array will be released back to space. Large negative spacecraft potentials will not result, and if electrons are freely released, the situation on the left in Figure 1 will result.

Figure 2 represents experimental data for a solar array section biased positive with respect to the plasma in which it is immersed [2]. The left half of the figure illustrates that at voltages greater than approximately 100 V, the electron current

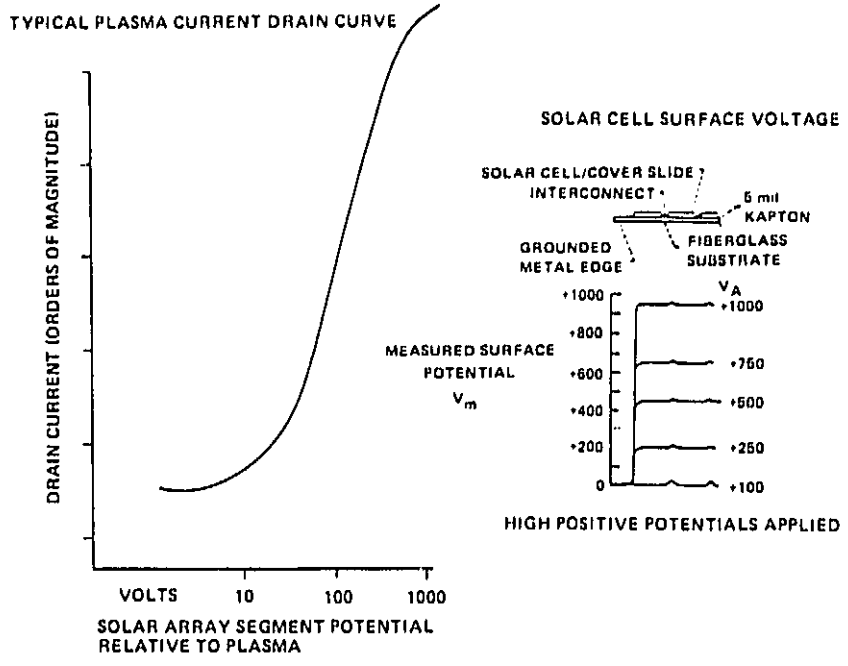

Figure 2. Solar array section biased positive relative to plasma environment.

collected by the solar array increases dramatically. The right half of the figure illustrates why. Even though the solar array surface is dielectric, the surfaces become highly positive and collect current as though the whole surface was a conductor. The explanation appears to be that as the plasma sheath grows around exposed interconnects or pinholes, the accelerated electrons strike the dielectric and low-energy secondary electrons are released which are collected by the exposed metal. This leaves the dielectric cover glass positive, allowing the plasma sheath to grow over the solar cells [3]. Therefore, the solar array can collect electrons as though it was all conductor. As the voltage on the array segment and the effective collection area increases, the amount of current collected rises, as indicated in Figure 2. This current flow through the plasma is current which is not available to the spacecraft and therefore represents a power loss to this plasma shunt. Depending on the solar array voltage, the power loss can be substantial and can seriously impact array performance.

No direct measure of the power loss exists because essentially all data consist of currents of charged particle collected by solar array segments with a potential impressed on them by a power supply. The power loss, which will be experienced in a solar array due to the collection of charged particles from the plasma, has at times been estimated by multiplying the collected solar array segment current by the voltage between the solar array segment and the plasma and summing over the segments. Such an estimation does not consider the current flow in the solar array. A solar array which is not in a plasma environment will have only the load current flowing in it. The current is the same throughout the array and the array can be operated at its maximum power point. However, a high voltage solar array immersed in a plasma will collect plasma current which will flow through the array in addition to the load current. The plasma current collected at a location on the array is a function of the potential between that location on the array and space. The current flowing through a specific point in the array is the load current and the sum of electron currents collected at points in the array at higher positive voltages. Therefore, nonuniform currents will flow within the array. To operate at the solar array average maximum power point, each individual cell will operate off its individual maximum power point, additionally degrading performance.

In the past ground tests, a uniform voltage was impressed on test samples and the collected charged particle current from the plasma measured. However, for a solar array which is generating its own voltage by having solar cells placed in series, there will be voltage gradients on the surface of the cells due to difference in voltage between cells. The gradients may be quite high if the cells are strung such that solar cells at considerably different voltages lie next to each other. Figure 3 shows a typical pattern for series connection of solar cells. Such a pattern minimizes current-induced magnetic fields. However, as evident in Figure 3, this layout of solar cells and electrical modules leads to the largest surface voltage gradients since the potential extremes lie adjacent to each other. The electric field structure in the plasma sheath may be complex due to solar cell layout and may influence charged particle collection. If electrons, influenced by the surface voltage gradient, are actually collected at the higher positive potentials, the power loss will increase accordingly.

A discharge phenomenon around the solar array has also been observed in some ground tests [4]. In these cases a bright glow appeared around the solar array and the electron currents collected by the solar array from the plasma increased by orders of magnitude. Such an increase in current will substantially affect the power loss in the solar array.

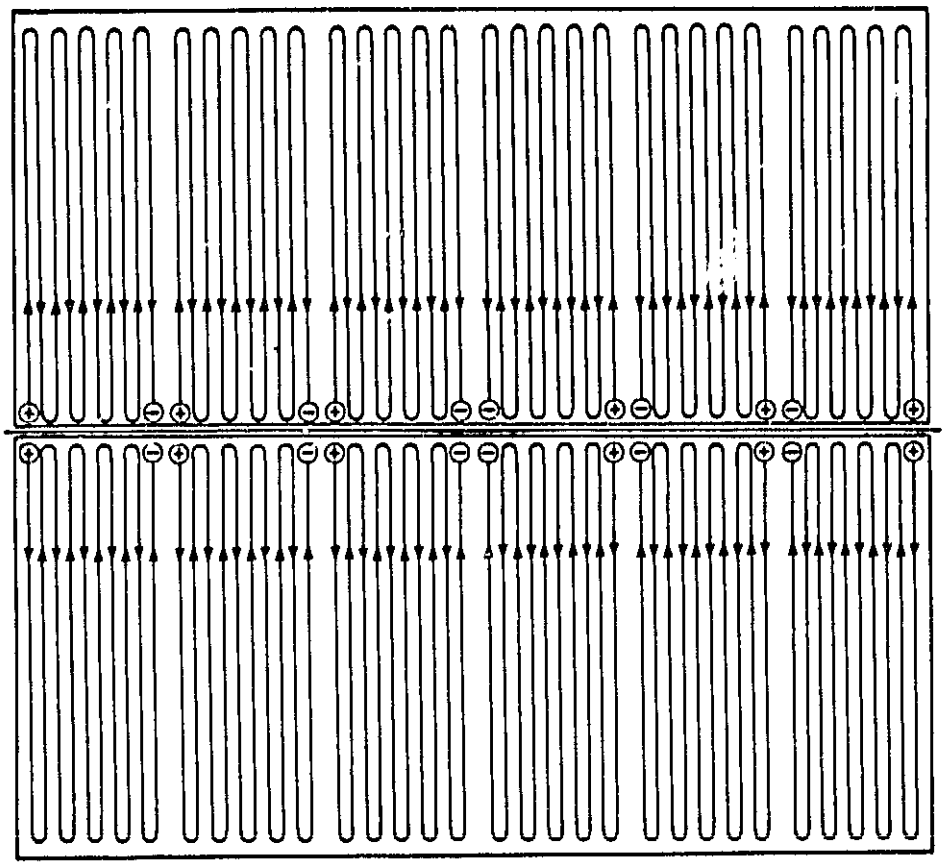

Figure 3. Typical pattern for series connection of solar cells to minimize magnetic field.

As previously pointed out, the collection of charged particles from the plasma and determination of how this affects solar array performance is a complex problem. It may be complicated by how voltage gradients on a solar array surface affect charged particle collection. A previous study by Suh and Stauber addressed whether surface potential gradients on solar arrays in geostationary orbit conditions might affect solar array performance [5]. Their conclusion was that the surface gradient will affect electron collection but that the magnitude of the currents in these plasma conditions is small enough so that their impact on array performance is negligible. Because of the much higher plasma densities in low Earth orbit relative to geosynchronous orbit, voltage gradients on the solar array surface may affect array performance. There has been no previous examination of plasma sheath growth around or charged particle collection from a plasma of ionospheric density by solar array or pinholes when a voltage gradient is present. This paper reports on experimental work addressing this subject.

THEORETICAL BACKGROUND

A large amount of experimental work regarding charged particle collection by both pinholes in dielectrics and segments of photovoltaic cells has been performed. The pinhole investigations have been conducted in order to understand the physics

involved in charged particle collection by high voltage solar arrays immersed in a plasma. The first experiments to examine high voltage solar array/space plasma interactions and identify an anomalously high electron collection was performed by Kennerud [6]. A large number of subsequent experiments investigated the same phenomenon and tried to determine the cause for the large current collection for samples biased positively of the ambient plasma and to determine the effect such current collection has on solar array performance.

Data on current collection and surface potential of both biased solar array segments and pinholes in dielectric material backed by biased electrodes indicate that the plasma sheath grows over the dielectric surface for positive potential relative to the plasma. This is observed not to be the case for negative potentials when ions are collected [2]. It has been postulated that as the sheath begins to grow around the exposed metal, incoming electrons strike the dielectric surface and low-energy secondary electrons are released and collected, leaving the surface positive. Analytical examination of charged particle collection by pinholes provides qualitatively correct comparison with experiment [7]. A key to this analytical examination is consideration of secondary electron production.

Previous work has been associated with a single bias voltage on a single pinhole or segment of solar cells. In order to determine the effects of a surface voltage gradient, multiple exposed conductors at different voltages surrounded by dielectric must be examined. If the sheaths which develop around the exposed conductors overlap, then a potential gradient will exist across the surface and within the sheath. Secondary electrons are low energy, therefore, a small potential gradient can move these electrons farther away to a higher potential point. Electrons which would have been collected at a lower potential will be collected at a higher potential.

In order to predict how charged particles are collected for multiple pinholes or openings in insulation, the plasma sheath structure must be known. The only experimental examination of sheath structure around pinholes was performed by Gabriel, et al. [8]. They determined that simple Debye shielding cannot describe the sheath structure but that it may be satisfactorily described as having an exponential drop-off with characteristic lengths in the z and r axes where the r axis is radially across the dielectric surface from the pinhole and the z axis is perpendicular to the dielectric surface. According to Gabriel, et al., the potential structure may be described by the semi-empirical formula,

$$\phi(r,z) = \frac{2\,\phi_o}{\pi}\,\tan^{-1}\left[\frac{a}{z}\exp\left(-\frac{z}{\alpha}\right)\right]\exp\left(-\frac{r^2}{\lambda^2}\right) \qquad (1)$$

The potential at any point in space due to two pinholes is given by the sum of the potentials due to the pinholes at that point. Figure 4 illustrates the geometry for such such a case. Using this figure;

$$\phi(r_3,z) = \frac{2\,\phi_2}{\pi}\,\tan^{-1}\left[\frac{a}{z}\exp\left(-\frac{z}{\alpha_1}\right)\right]\exp\left(-\frac{r_3^2 + d^2 - 2r_3\,d\cos\theta}{\lambda_1^2}\right)$$

$$+\frac{2\,\phi_2}{\pi}\,\tan^{-1}\left[\frac{a}{z}\exp\left(-\frac{z}{\alpha_2}\right)\right]\exp\left(-\frac{r_3^2 + d^2 + 2r_3\,d\cos\theta}{\lambda_2^2}\right) \qquad (2)$$

for equivalent size pinholes separated a distance 2d.

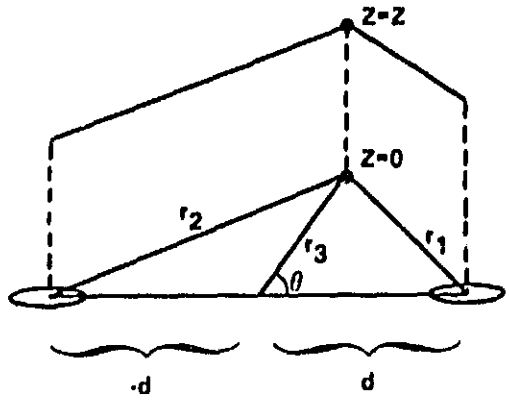

Figure 4. Geometry for potential distribution around two pinhole defects in insulator.

A simpler geometrical arrangement to consider is illustrated in Figure 5. Instead of pinholes, slits in a dielectric covering conductors are considered. This simplified the geometry considerably. In this case,

$$\phi(x,z) = \frac{2\,\phi_1}{\pi} \tan^{-1}\left[\frac{a}{z} \exp\left(-\frac{z}{\alpha_1}\right)\right] \exp\left(-\frac{x^2}{\lambda_1^2}\right)$$

$$+ \frac{2\,\phi_2}{\pi} \tan^{-1}\left[\frac{a}{z} \exp\left(-\frac{z}{\alpha_2}\right)\right] \exp\left(-\frac{(d-x)^2}{\lambda_2^2}\right) \qquad (3)$$

The values of ϕ, a, α, and λ are experimental parameters. Values of $\phi_{1,2}$ are set by the experiment. The values of a, α, and λ must be found by experimentally obtaining values of $\phi(x,z)$.

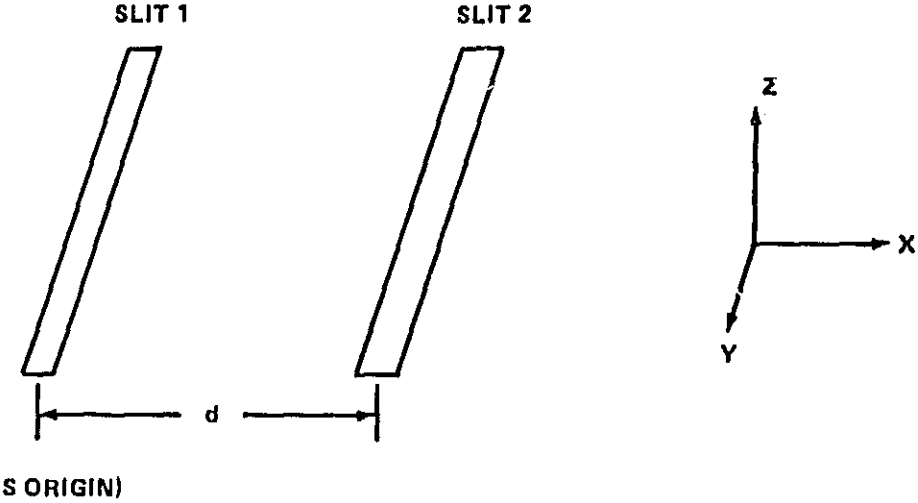

Figure 5. Geometry of potential distribution around two slits in insulator.

Using the experimental geometry described above, change in ϕ_z indicates the energy with which electrons are accelerated to the surface. Whether they are collected by one exposed conductor or the other depends on the radial electric field component given by,

$$E(x,z) = -\frac{\partial \phi(x,z)}{\partial x}$$

$$= \frac{2}{\pi}\left\{\frac{2x\ \phi_1}{\lambda_1^2}\tan^{-1}\left[\frac{a}{z}\exp\left(-\frac{z}{\alpha_1}\right)\right]\exp\left(-\frac{x^2}{\lambda_1^2}\right)\right.$$

$$\left. -\frac{2(d-x)\ \phi_2}{\lambda_2^2}\tan^{-1}\left[\frac{a}{z}\exp\left(-\frac{z}{\alpha_2}\right)\right]\exp\left(-\frac{(d-x)^2}{\lambda_2^2}\right)\right\} \qquad (4)$$

This equation shows that there is a mild dependence of $E(x,z)$ on z but that it is dominated by x. Equation (4) may be used to find the point at which the x-axis component of the electric field is zero, or where the electric field direction reverses. If this field reversal point is between the two slits, it will establish the boundary which will determine that charged particles entering on one side of it will be collected by the other. If the potential difference and proximity of the slits are such that the field reversal point is at or near one of the slits, all the charged particles entering between the slits may be collected by the higher potential slit.

As the plasma sheath develops around each individual slit, the sheaths are independent. If the potential on an individual slit is raised such that the sheath boundary extends beyond the point halfway between the two slits, a certain amount of current is collected. If the potential on the second slit is raised until the sheaths overlap, the charged particles collected by the high potential slit will include charged particles which would have been collected by the lower potential slit. However, the total current should be less than if the two slits were removed from each other and kept at the same potentials relative to the plasma. This is because the sheath area of the two removed sheaths is greater than the case when the sheaths coalesce.

EXPERIMENTAL APPARATUS

The apparatus for this experiment consists of a vacuum chamber, plasma source, plasma diagnostics, and test articles. The steel vacuum chamber is approximately 1-m diameter by 2-m long. Two 12-in. diffusion pumps provide a pressure of approximately 1.0×10^{-6} torr when the plasma source is not operating. The background neutral pressure is maintained in the 10^{-5} torr range during plasma source operation; its exact value dependent on gas flow rate through the plasma source.

The plasma source chosen is a hollow cathode plasma source which is based on the design reported by Kaufman and Robinson [9] and Stillwell, et al. [10]. The hollow cathode design was chosen for several reasons. The hollow cathode design requires fewer power supplies than other alternatives and does not require a filament

cathode which has a limited lifetime. Also, the hollow cathode can more easily offer a higher ionization efficiency than an electron bombardment device.

The design of the hollow cathode is illustrated in Figure 6. The working gas in this experiment is argon. The gas is allowed to flow into the body of the source and into the interior of the tantalum tube. This tube is 5.5-cm long, 0.64 cm in diameter, and has a wall thickness of 0.051 cm. The insert is formed by rolling a strip of 0.0254-mm tantalum foil which is 1-cm wide. Similar rolls of tantalum foil on the outside of the tantalum tube act as a radiation shield. The starter electrode is used to initiate a discharge within the hollow cathode between the electrode and the insert. The electrode is made of a 0.051-cm diameter tungsten rod embedded in a ceramic rod. The tip of the hollow cathode is made of carbon, machined to fit into the end of the tube. The carbon tip has a 1.0-mm orifice centered in it through which the gas and electrons exit the cathode. The anode is composed of a roll of stainless steel wire mesh which is about 5.5 cm in diameter and 9.0-cm long. The anode is flush with the tip of the cathode. They are shown separated in Figure 6 for clarity.

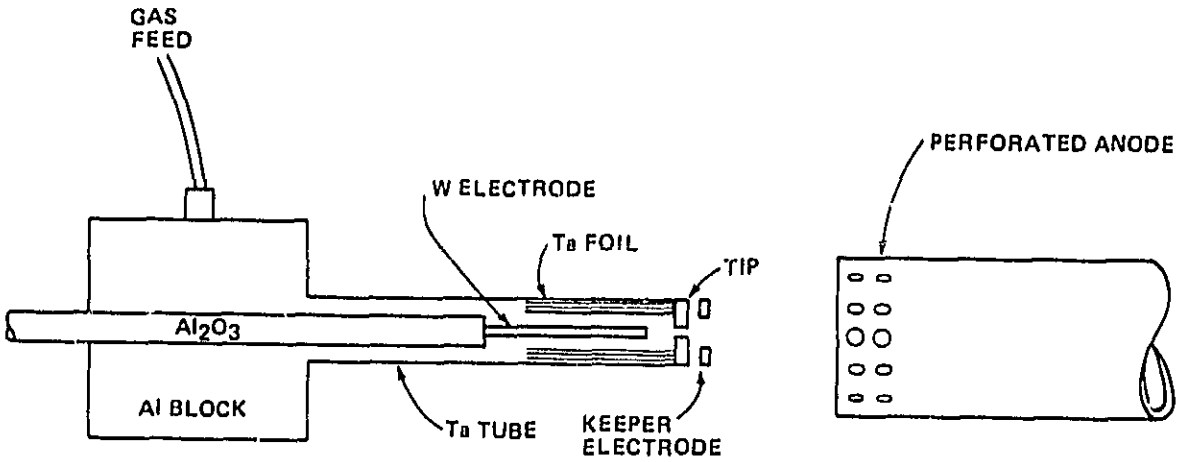

Figure 6. Diagram of hollow cathode plasma source.

Typically, hollow cathodes make use of an insert doped with a low work function material for easy electron emission. The difficulty with their use in a laboratory condition is that they must be conditioned before use and, if they are exposed to atmosphere, the emitter becomes poisoned and must be reconditioned or replenished. The design chosen utilizes an undoped tantalum foil insert and is, therefore, not sensitive to repeated opening of the test chamber. The starter electrode is used to initiate a discharge inside the hollow cathode. Once the tantalum foil is heated to the point that it will support thermal emission (normally a matter of seconds) and the internal discharge is able to couple from the cathode to the anode, an arc discharge is initiated and the starter electrode turned off.

The keeper electrode aides in coupling the electrons from the internal discharge through the orifice in the cathode to initiate the arc discharge to the anode. Once this discharge is established, the keeper electrode power supply is also turned off.

A Langmuir probe is used to determine the characteristics of the plasma generated by the plasma source. The probe is placed in the proximity of the test article so that the plasma conditions at the test article are known. The probe consists of a 7.5 cm long tungsten wire which is 0.051 cm in diameter. The length is

chosen to minimize end effects and the diameter insures the capability of using thick sheath analysis of the probe data. Data were obtained by sweeping the probe potential both negative and positive of the plasma potential and measuring the collected current. Analysis of the resulting current/voltage curve allows determination of the electron temperature, electron density, and plasma potentials.

Two emissive probes are used to determine the local potential within the plasma sheath which develops around the slits in the test article. The probes each consist of a loop of wire. Tungsten/rhenium wire 0.076 mm in diameter and forming a loop 1.5-mm wide and 1.5-cm long is used in this experiment. A current is passed through the wire which heats it to incandescence. If the probe is allowed to electrically float, it will come to a potential near plasma potential by thermal emission of electrons. As with the Langmuir probe discussed above, a complete current-voltage curve can be obtained and the plasma information determined. Based on the work of Aston and Wilbur [11] and Gabriel et al. [8], it is sufficient to allow the probe system to float and obtain one curve of the probe voltage as a function of filament current. The current at which the electron saturation point is reached can, therefore, be determined. Then, the probe can be maintained at this filament current and used to determine local potential. Figure 7 illustrates the circuit used in this experiment.

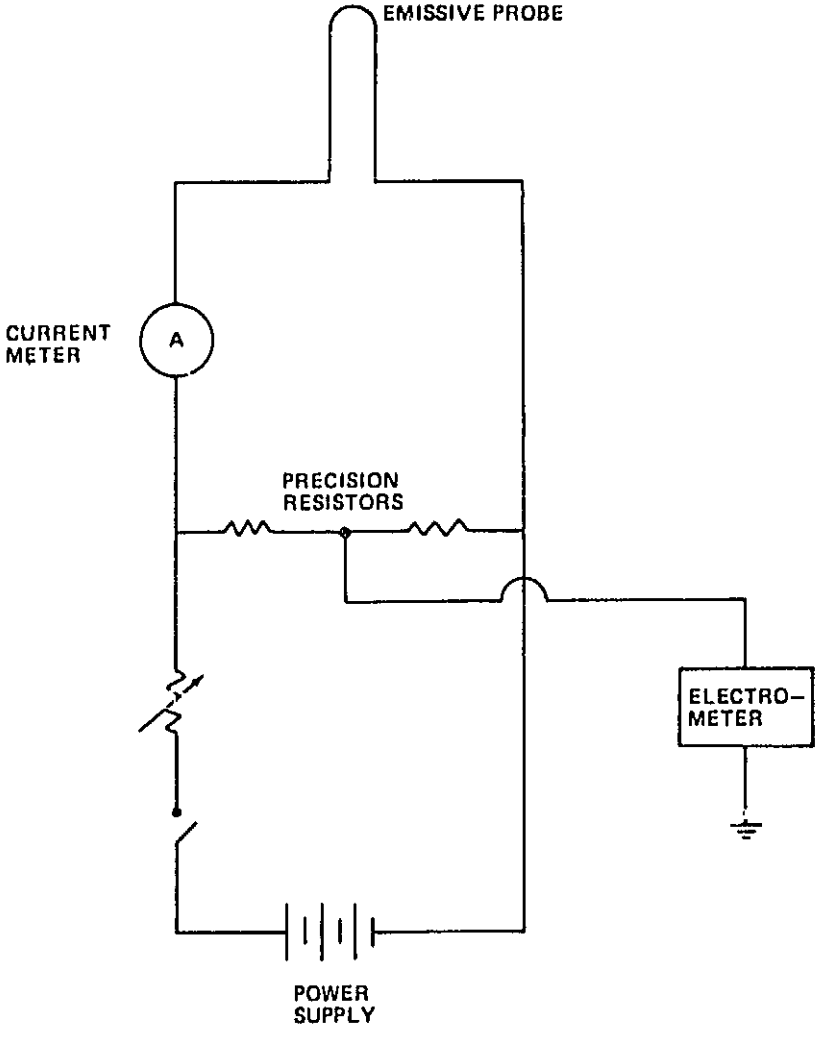

Figure 7. Emissive probe circuit.

In the experiments described in this report, the noted filament currents are obtained and the emissive probe passed through the outer regions of the plasma sheath formed around the slits. This allows a determination of the radial variation in the sheath potential for the set axial distances of the two probes.

The test article consists of a 232-cm^2 printed circuit board covered with 2.0-mil kapton sheet containing open slits. Data were collected on two slit configurations. In one, the slit widths were 0.64 cm and the slit spacing, d, was 3.0 cm. In the other case, the slit widths were 0.32 cm and the slit spacing, d, was 2.0 cm. The metal electrodes are copper and their pattern is shown on Figure 8. The kapton sheet with the proper slits is overlaid on the circuit board and is held by small retainers around the kapton perimeter. The electrical connections are made through the back of the circuit board. Figure 8 also illustrates the slit configuration when kapton sheet is applied to the circuit board.

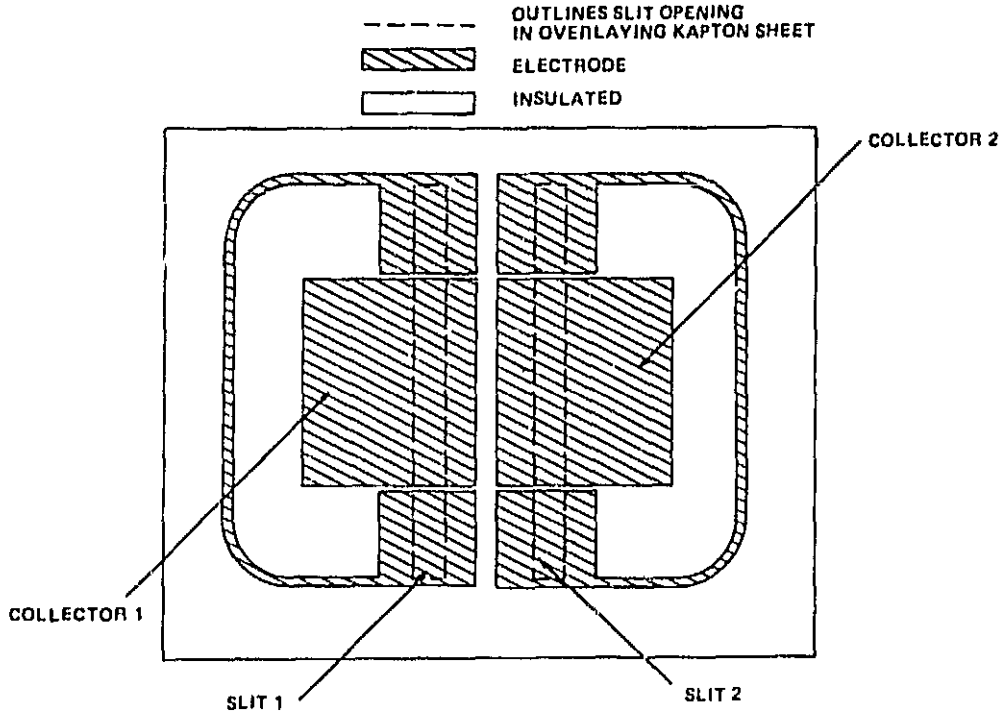

Figure 8. Test article electrode pattern on printed circuit board.

The conductor pattern shown in Figure 8 facilitates data collection from slits in the kapton. The electrodes on each end of the center electrodes are maintained at the same potential as their respective center electrode. However, current measurements are obtained only from the center electrodes. This way the data are obtained with a uniform sheath structure along the length of the center electrode and fringing field effects at the ends of the slits do not affect the data. The length of the slit from which current data are collected is 4.22 cm.

Figure 9 indicates the placement of diagnostic probes around the test article. The slit geometry allows the emissive probes to have a scale length small compared to the sheath size. In a circular or spherical geometry, a much smaller, more delicate probe size would be required for the same scale length.

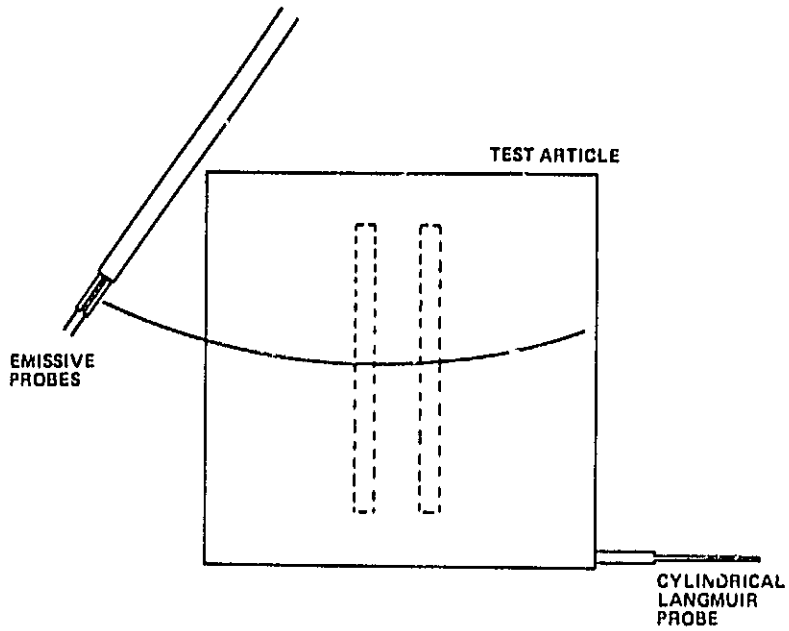

(a)

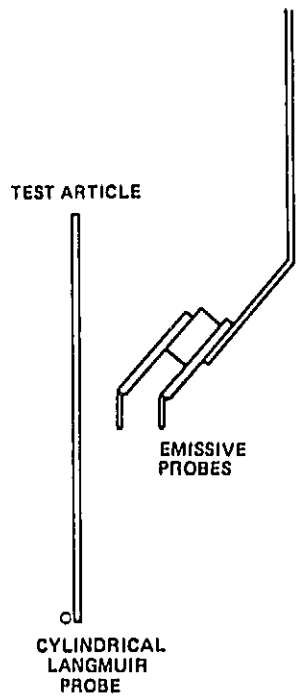

(b)

Figure 9. Test article and diagnostic probes.

EXPERIMENTAL RESULTS

Plasma Conditions

Data were obtained for slightly different plasma conditions. In one case, the gas flow rate through the plasma source was 1.0 A equivalent, meaning that if the gas was fully ionized, 1 A of ions exit the plasma source orifice. The plasma source was operated at a discharge current of from 3.0 to 5.0 A and the voltage allowed to vary. Repeated operation of the source and collection of data indicate that by setting the plasma source operating conditions, the plasma conditions are reproduced with minimal variation. The plasma conditions are obtained with the cylindrical Langmuir probe. The plot of the logarithm of the current versus probe voltage in the region of the electron retarding-acceleration transition provides the electron temperature. For a cylindrical Langmuir probe when the thick sheath approximation is valid, the current squared versus the probe voltage in the acceleration region is a linear relationship. The electron density of the plasma may be found by [12]

$$n_e = \left(\frac{\pi^2 \, S \, m_e}{2 \, A_p^{\,2} \, e^3} \right)^{1/2} \tag{5}$$

where s is the slope of the current squared versus voltage curve. Data were obtained for Ar gas flows of from 0.5 to 1.0 A equivalent. This variation provided plasma temperatures of from 2.0 to 3.0 eV and plasma densities of from 2 to 4 x 10^6 electrons cm^{-3}. It should be noted that the error expected in determining the density values given is considered to fall within the experimental error of each other. Even though the absolute values are not distinguishable, the relative values are apparent because increased current collection by the slits is observed for greater gas flow through the plasma source.

Sheath Structure Around Slits

The emissive probes, previously described, are used to determine the sheath structure around the pair of slits which are 0.64-cm wide and 3.0-cm apart. These probes will be referred to as the inner and outer probe for the one nearest and farthest, respectively, from the test sample. As already described, the filament current versus probe potential relative to ground is obtained in the plasma near the test sample. The resulting curves are shown in Figure 10. As can be seen, the emissive probes reach plasma potential with a filament current of 0.6 A. Therefore, the filament current can be set to 0.6 A and the emissive probe used to measure local plasma potential.

First, the potential structure of the sheath around individually biased slits was measured and subsequently the structure of the sheath due to biases on both slits was measured. The sheath structure around individual slits is symmetrical about their center. It is observed that for both slits biased, the structure of the sheath in the region of the highest potential slit, and which is not between the two slits, is the same as the single slit sheath. Therefore, no data of the sheaths of single slits are presented since this information can be obtained from the sheath data when both slits are biased.

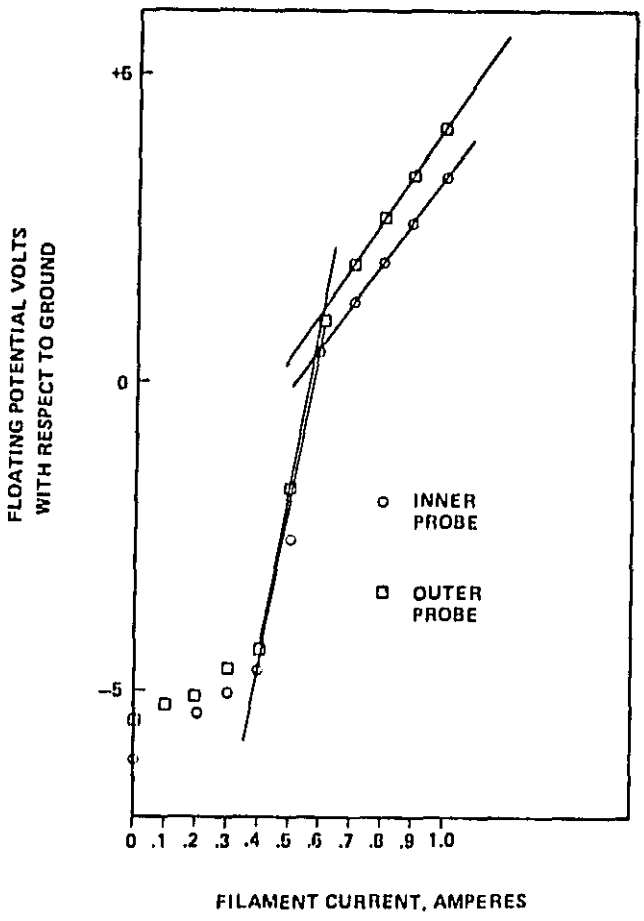

Figure 10. Emissive probe filament current versus floating potential.

Data for the potential structure at the location of the inner probe are given in Figure 11. Similar data for the outer probe location are given in Figures 12 and 13. It is evident from this data that the electric fields are strong within the sheath and that the merging of sheaths of the two slits is more evident in the sheath outer region. The position between the slits where the potential is a minimum defines the x axis electric field reversal point. Electrons which enter the sheath on one side of this point or the other will not likely cross the potential barrier and will be directed by the electric field to the slit on the electron side of the barrier. It can be seen in the data in Figures 12 and 13 that the position of the potential minimum shifts toward the slit with the lowest bias when the difference in bias between the slits increases.

The sheath structure around the slits for the different plasma source operating conditions is almost indistinguishable. A slightly greater potential penetration is observed for lower density. As will be shown, greater currents are collected for the higher plasma density condition. Calculation of the Debye length for the plasma cases shows that they have nearly the same Debye length and, therefore, characteristic shielding distances. With this in mind, the data are reasonable.

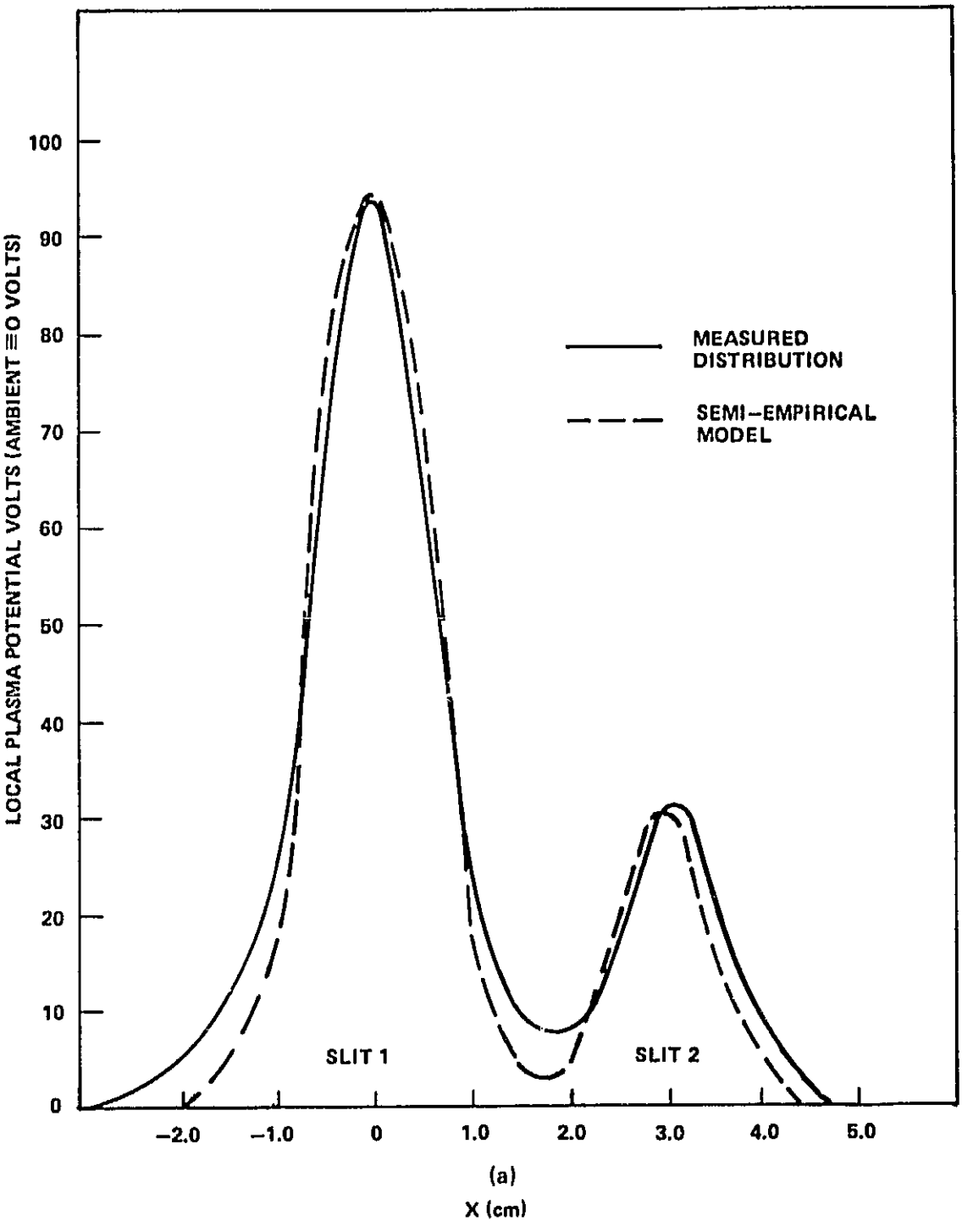

Slit width, 0.64 cm; slit separation, 3.0 cm; slit 2 at +128 V; slit 1 for (a) +328 V, for (b) +228 V, and for (c) +128 V.

Figure 11. Plasma sheath structure for inner probe Z axis location and 1.0 A equivalent gas flow.

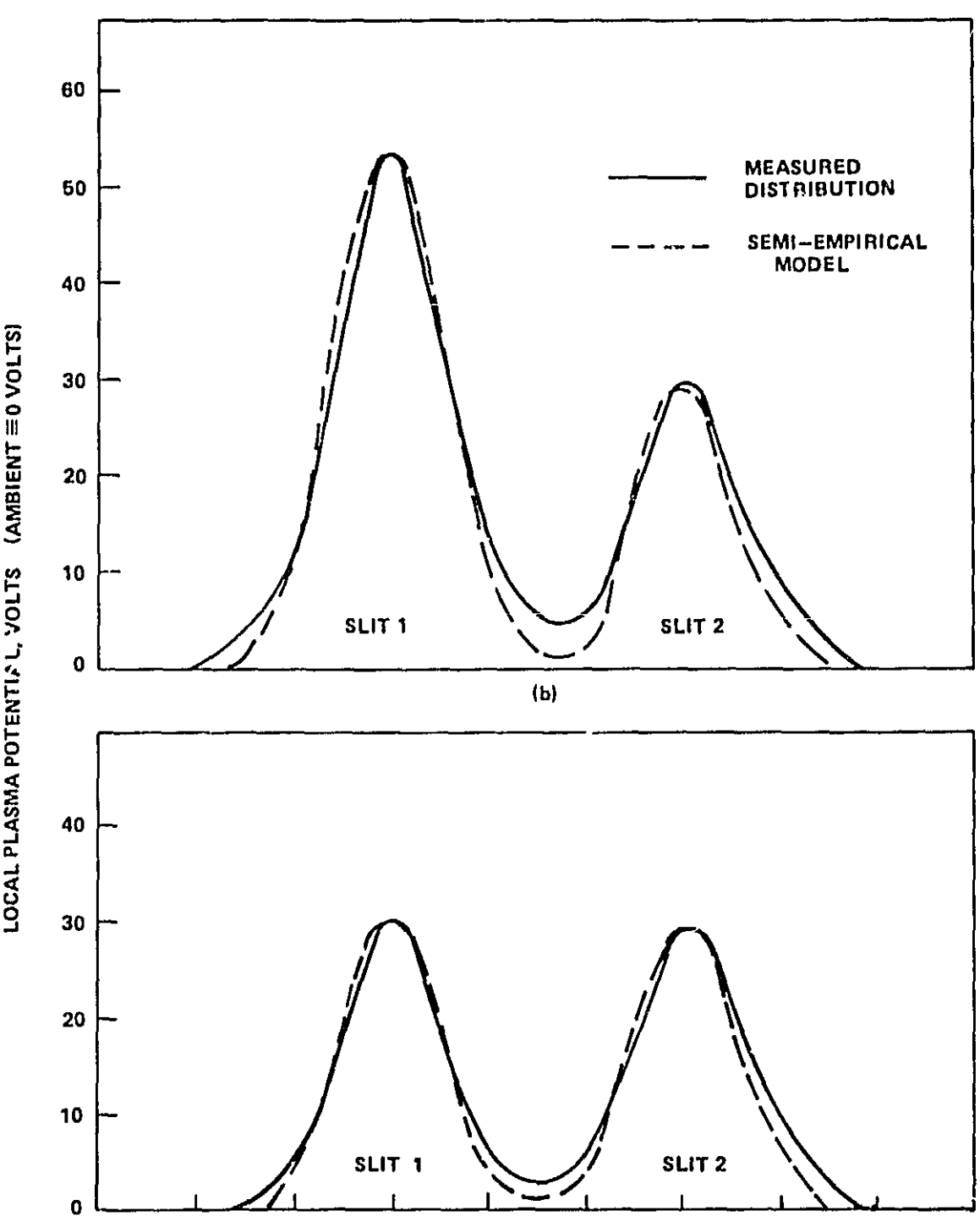

Figure 11. (Concluded)

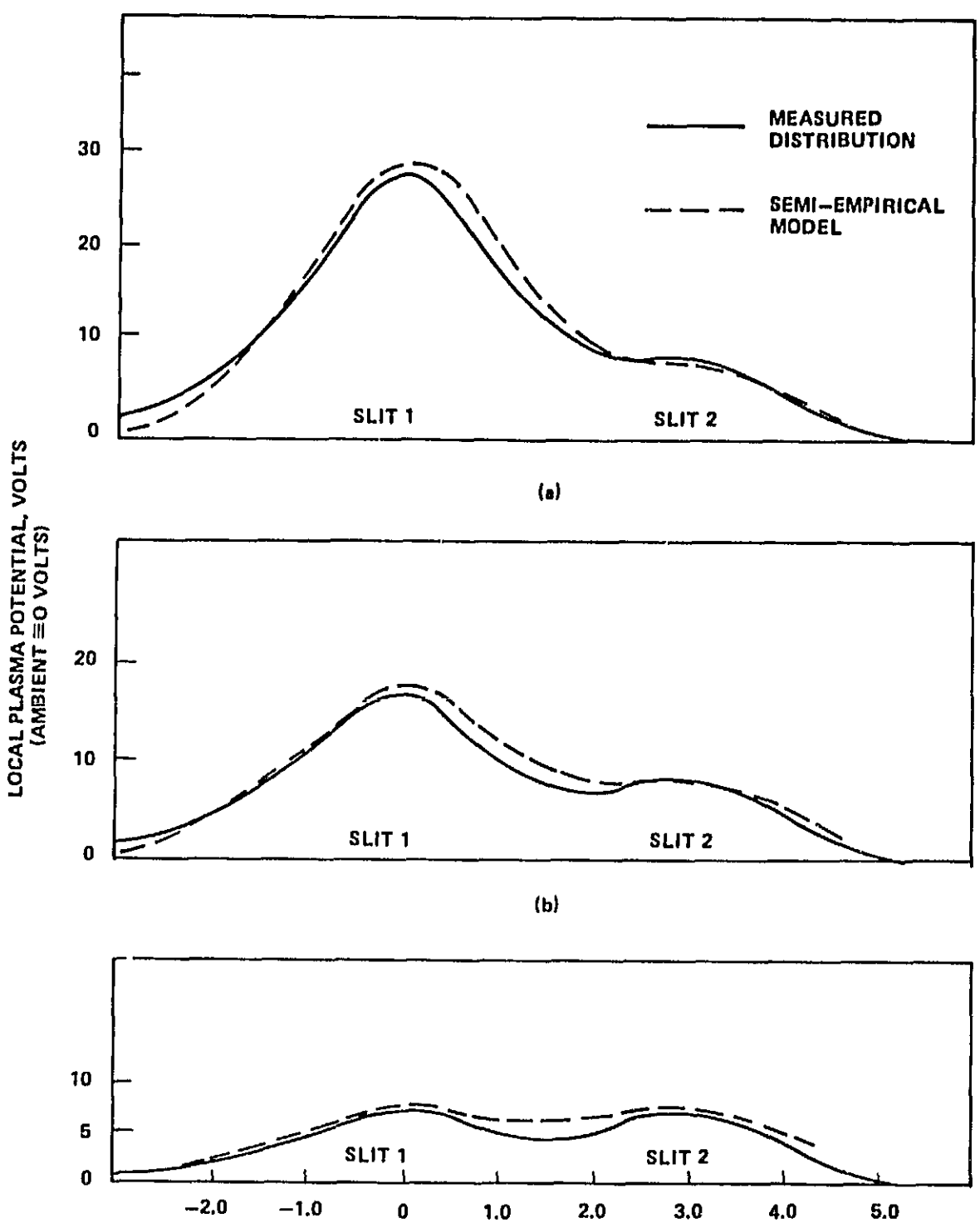

Slit width, 0.64 cm; slit separation, 3.0 cm; slit 2 at +128 V; slit 1 for (a) +328 V, for (b) +228 V, and for (c) +128 V.

Figure 12. Plasma sheath structure for outer probe Z axis location and 1.0 A equivalent gas flow.

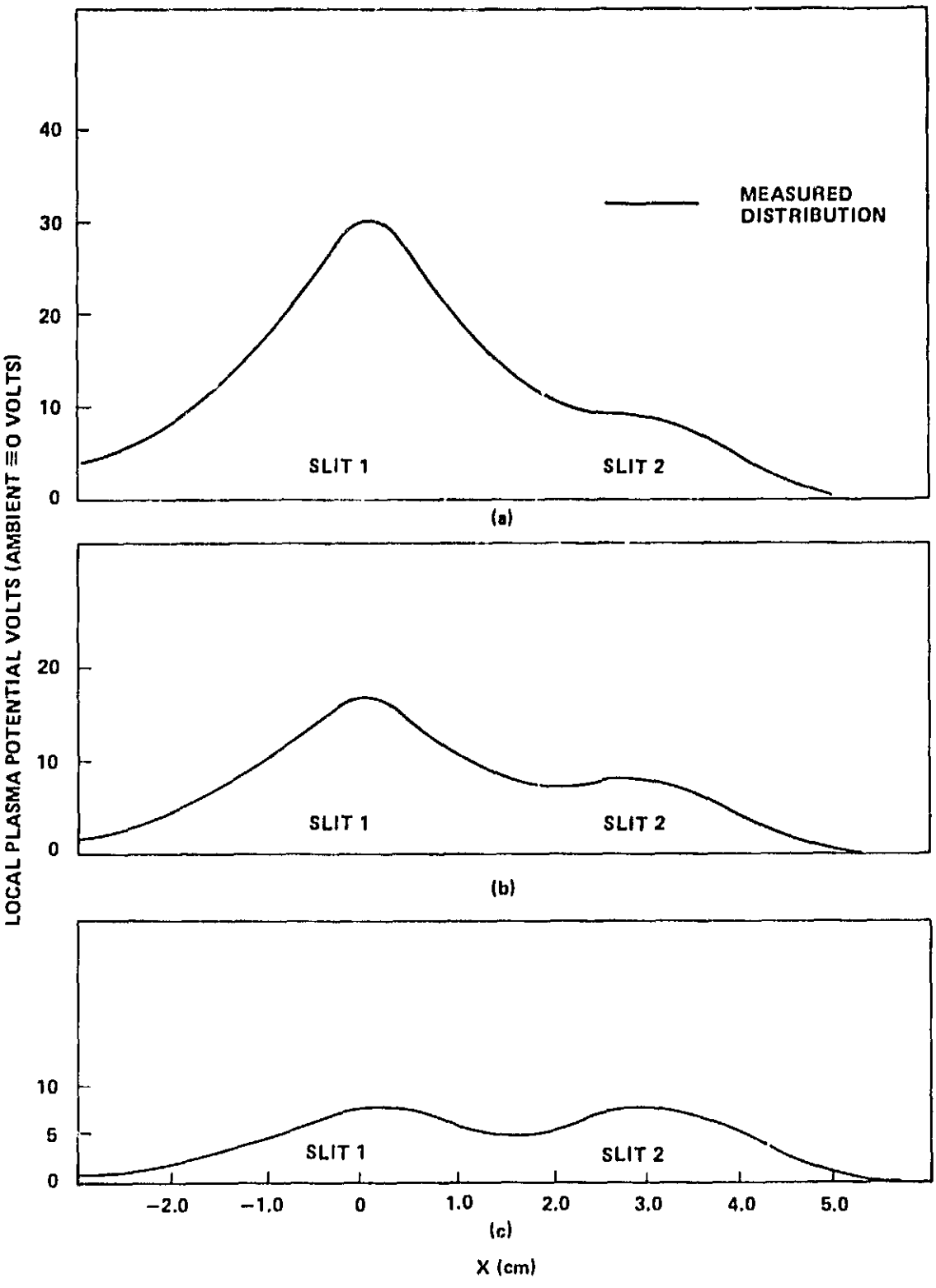

Slit width 0.64 cm; slit separation, 3.0 cm; slit 2 at +132 V; slit 1 for (a) +332 V, for (b) +232 V, and for (c) +132 V.

Figure 13. Plasma sheath structure for outer probe Z axis location and 0.5 A equivalent gas flow.

The data were utilized to find the values of a, α, and λ for each of the curves. They are given in Table 1 for the curves shown in Figures 11 through 13. Gabriel, et al. [8] indicated that a value of α and λ can be used to describe the potential structure throughout the sheath. However, as can be seen in Table 1, the measured values of λ do vary. Reexamination of the data presented by Gabriel, et al., does indicate that λ varies by about 40 percent for a Δz of 1.1 cm. The data presented in this report vary more than this. The reason may be the higher plasma density of this experiment or effects due to a slit geometry. For a given voltage bias and location in a plane defined by a distance on the z axis, a value of λ can be used to describe the x axis potential distribution. The values of a, α, and λ given in Table 1 for a single biased slit are used in equation (3) to describe the total potential distribution for the case where both slits are biased. The results of this calculation are also given in Figures 11 through 13. As indicated by the figures, the potential structure can be described by equation (3), with the limitations cited.

TABLE 1. EXPERIMENTAL VALUES OF a, α, AND λ

	a (cm)	α (cm)	λ (cm)
1.0 A Equivalent Gas Flow			
+130 V	0.51	1.55	
z = 0.8 cm			0.70
z = 1.8 cm			1.62
+230 V	0.40	2.98	
z = 0.8 cm			0.77
z = 1.8 cm			1.56
+330 V	0.53	2.47	
z = 0.8 cm			0.81
z = 1.8 cm			1.45
0.5 A Equivalent Gas Flow			
+130 V	0.51	2.9	1.49
+230 V	0.57	1.86	1.51
+330 V	0.64	2.12	1.51
z = 1.8 cm			

Electron Current Collection

In the previous section, data were presented on the sheath structure around slits in the kapton sheet covering biased electrodes. The sheath structure was examined for single-biased slits and for both slits biased. Data were also obtained of the electron current collected by the conductor exposed in the slit. As pointed out earlier, the conductors are guarded and data on current collection are only

obtained from the center portion of the electrode which is 4.22-cm long. Data were obtained for the two slit configurations mentioned; slit widths 0.65 cm and 0.32 cm for slit separations of 3.0 cm and 2.0 cm, respectively. Data were also obtained for two gas flow rates, 0.6 A equivalent and 1.0 A equivalent. The data presented in this report are individual data sets, rather than averaged values. The data sets were reproducible overall to within approximately 20 percent by resetting plasma source flow rate and discharge current.

The current collection data were much more reproducible at lower voltages on the slits. It was observed that as voltage on the slit is slowly increased to near 250 to 300 V, the collected current dramatically "steps" to a higher value, as though a different collection mode existed. This was observed by Gabriel, et al., in their pinhole examinations. For consistency, the data on current collection, when both slits are biased, are acquired only when this step transition has not occurred. To illustrate this transition affect, the voltage applied to the individual slits was both slowly increased and increased in abrupt steps. Figure 14 represents data for an individually biased slit. With step voltage increases, the transition to the higher collection mode occurs between +100 and +150 V.

In order to determine the effects a voltage gradient in the sheath has on current collection by the two slits, data were collected for various cases where both slits were positive of the ambient plasma and where a potential difference between the two slits exists. This was accomplished by biasing one of the slits by a set potential and maintaining it. The potential on the other slit was then continually increased and the current collected independently by both slits was obtained for the various potentials. This data are presented in Figures 15 and 16 for the 0.64 cm slits at 0.6 A equivalent gas flow rate. In the data presented in this report, slit 1 is always held at a constant potential and the potential varied on slit 2. It is observed that as the slit 2 potential is increased from zero, the current collected by slit 1 increases. As the potential on slit 2 increases to a value near or exceeding slit 1, the current collected by slit 1 decreases; all the while the current collected by slit 2 increases. The data may be best interpreted by referring back to the figures of the plasma sheath structure. As expected, when the bias on both slits is the same, the potential minimum, and the electric field reversal point, lies exactly between the two slits. As the bias on one of the slits increases, the minimum potential point and electric field reversal point moves toward the slit with the lower potential. Therefore, electrons which would have been collected by this slit are now collected by the higher potential slit.

Data on current collection similar to that already shown are given in Figures 17 through 19 for the same slit size of 0.64 cm, but for the 1.0 A equivalent gas flow rate. The trends are the same as for the lower flow except that the magnitude of the collected currents has increased, indicating an increased plasma density. Data for the same plasma conditions and slit potentials are given in Figures 20 through 25 for slit widths of 0.32 cm and slit separation of 2.0 cm.

Because the electron collection is dependent on where the electron enters the sheath relative to the electric field reversal point, the sheath potential curves at the 1.8 cm z-axis position are of most interest. In Figures 12 and 13, the electric field reversal point is still distinguishable for the case of one slit bias about +230 V and the other +130 V. However, for the case of one slit bias about +330 V and the other maintained at +130 V, this point is becoming indistinguishable and one expects the amount of current collected by the higher potential slit to increase. Indeed, this can be seen in the data. Figure 11 indicates that slightly deeper in the sheath the

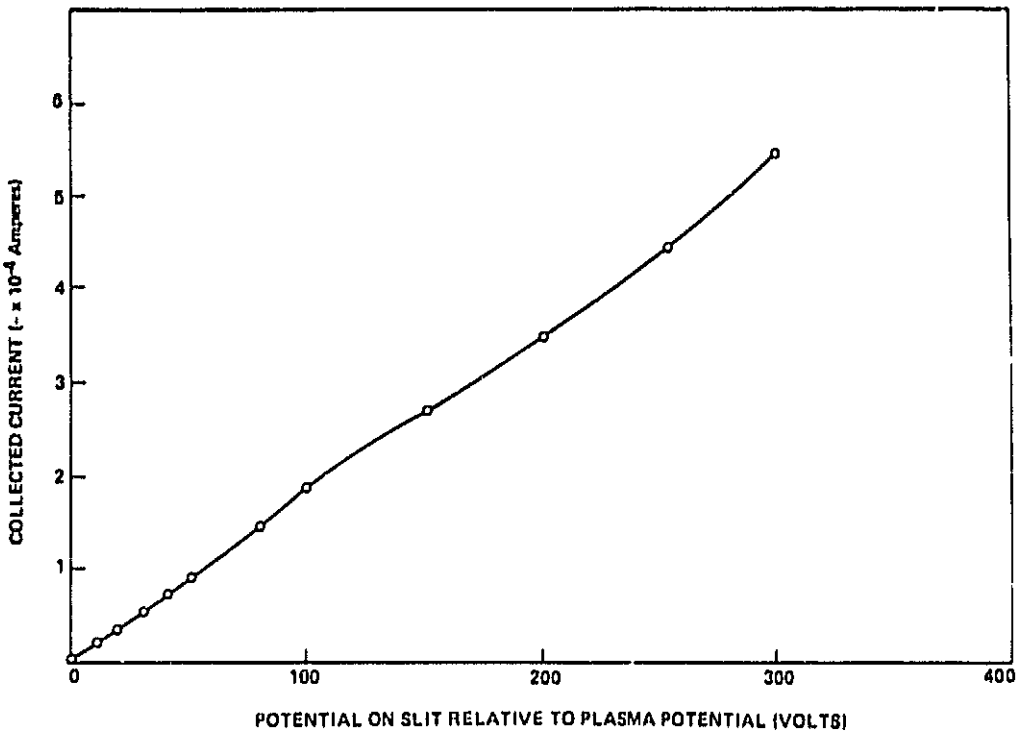

(a)

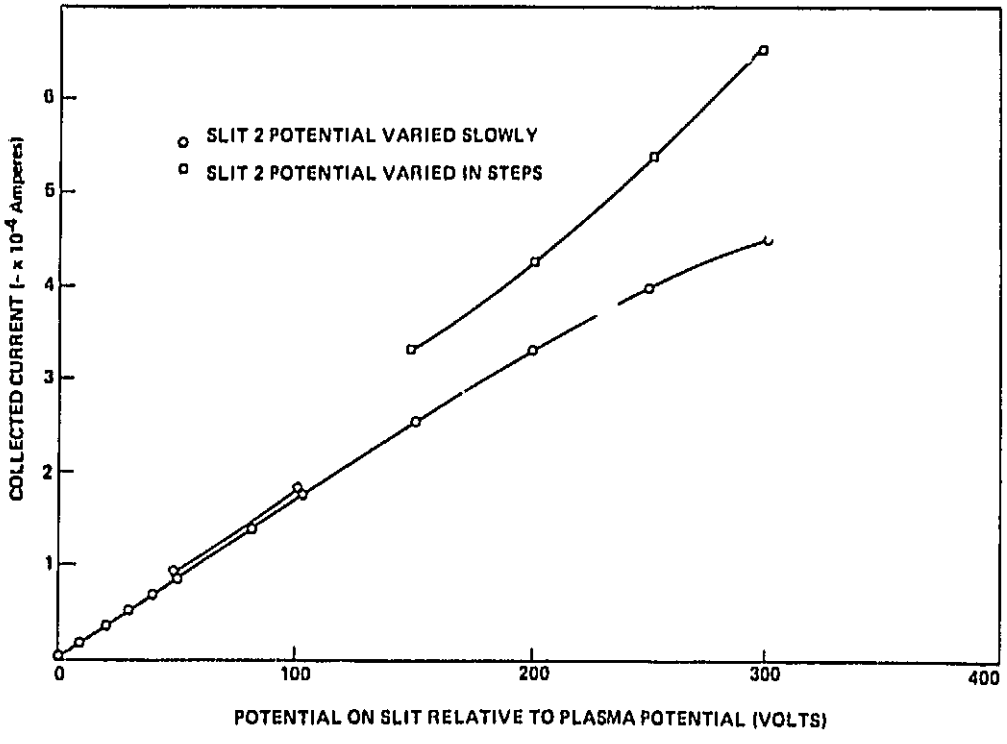

(b)

Figure 14. Current collected by single biased slit.

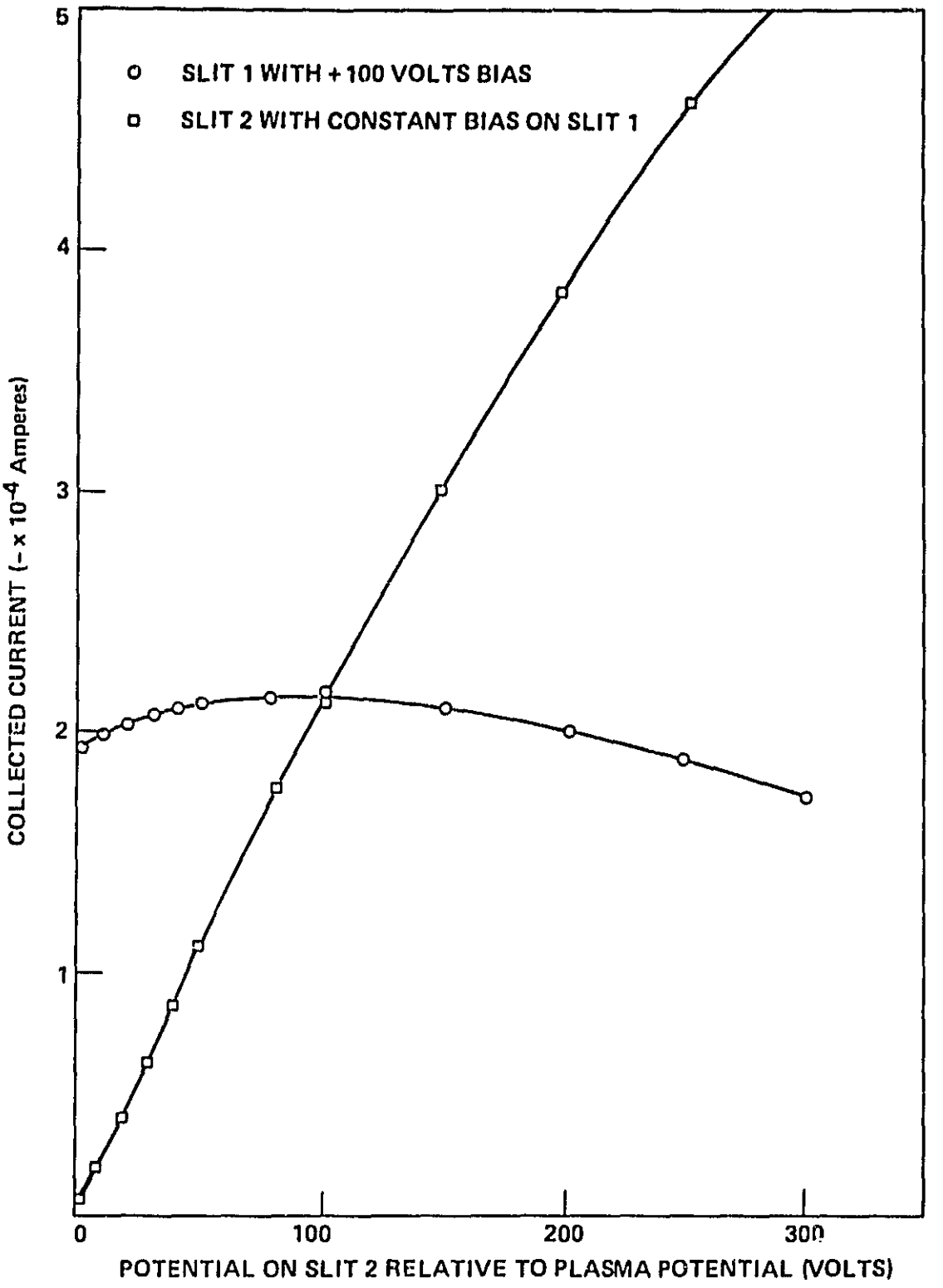

Figure 15. Current for two biased slits: One +100 V and the other varied.

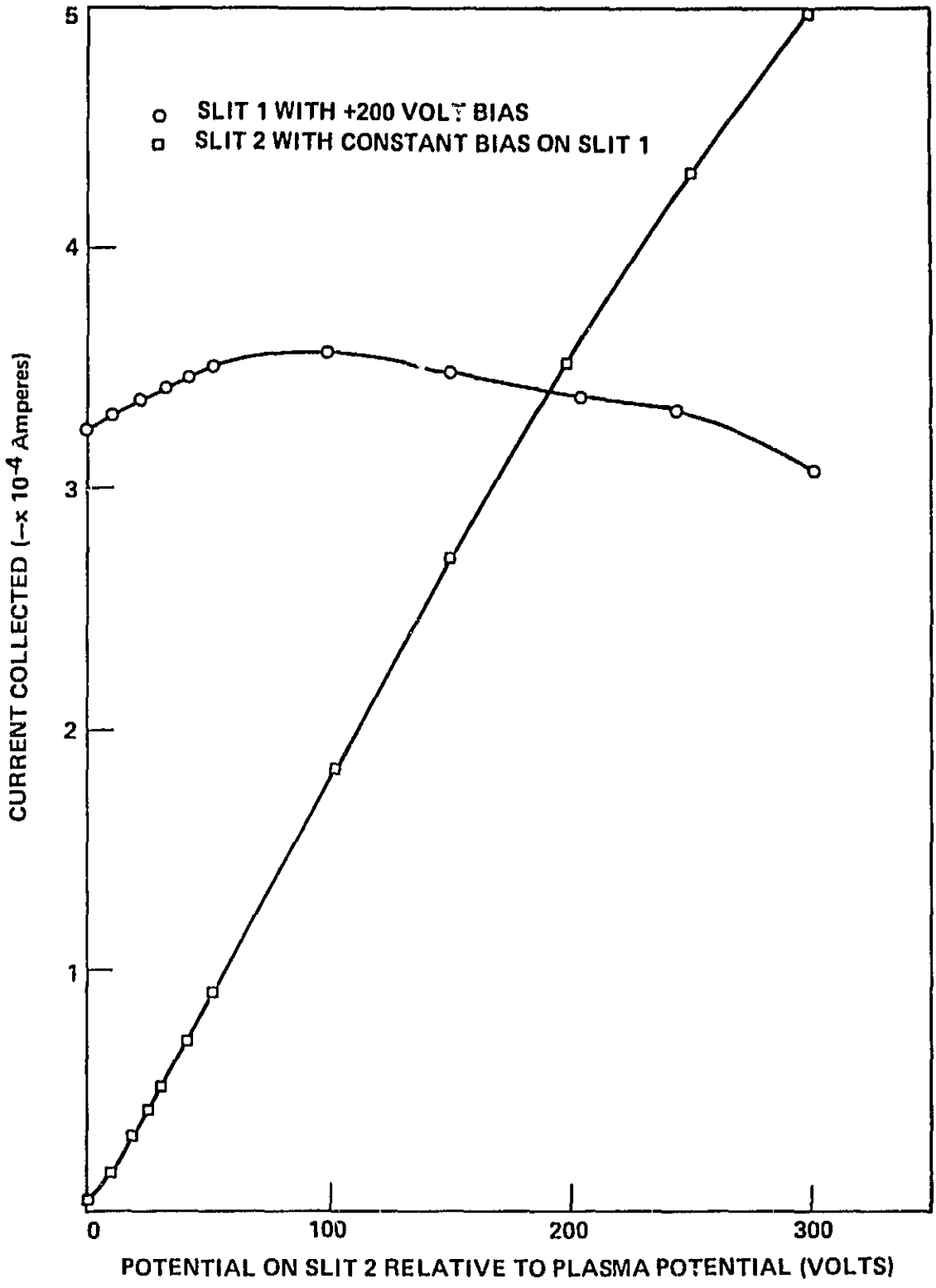

Figure 16. Current for two biased slits: One +200 V and the other varied.

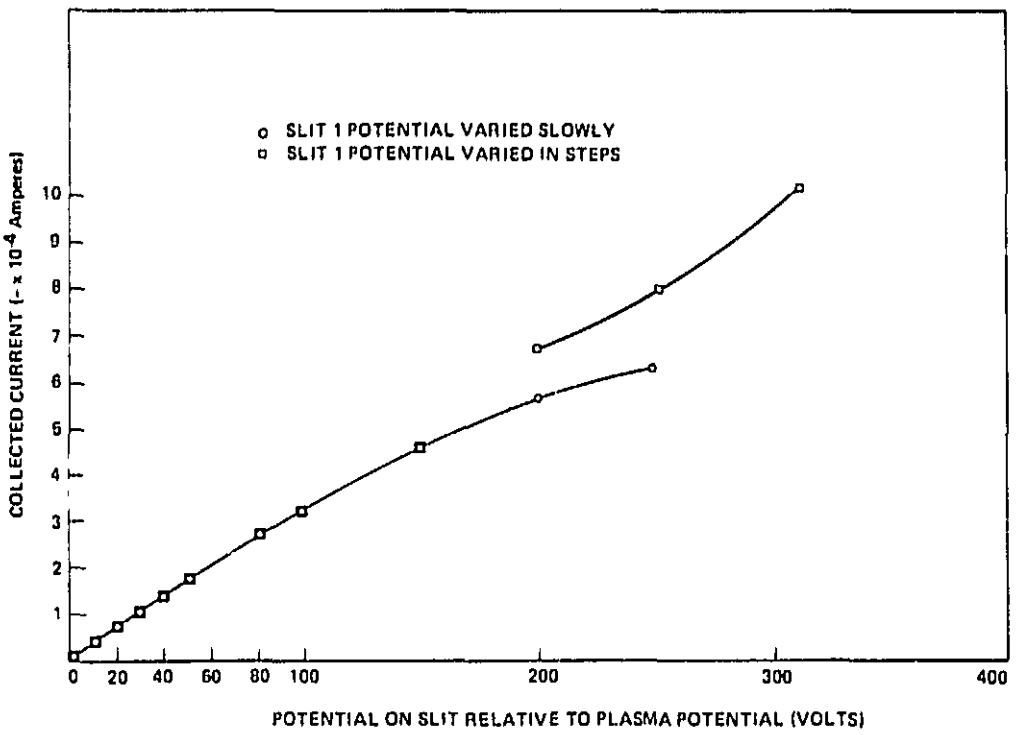

(a)

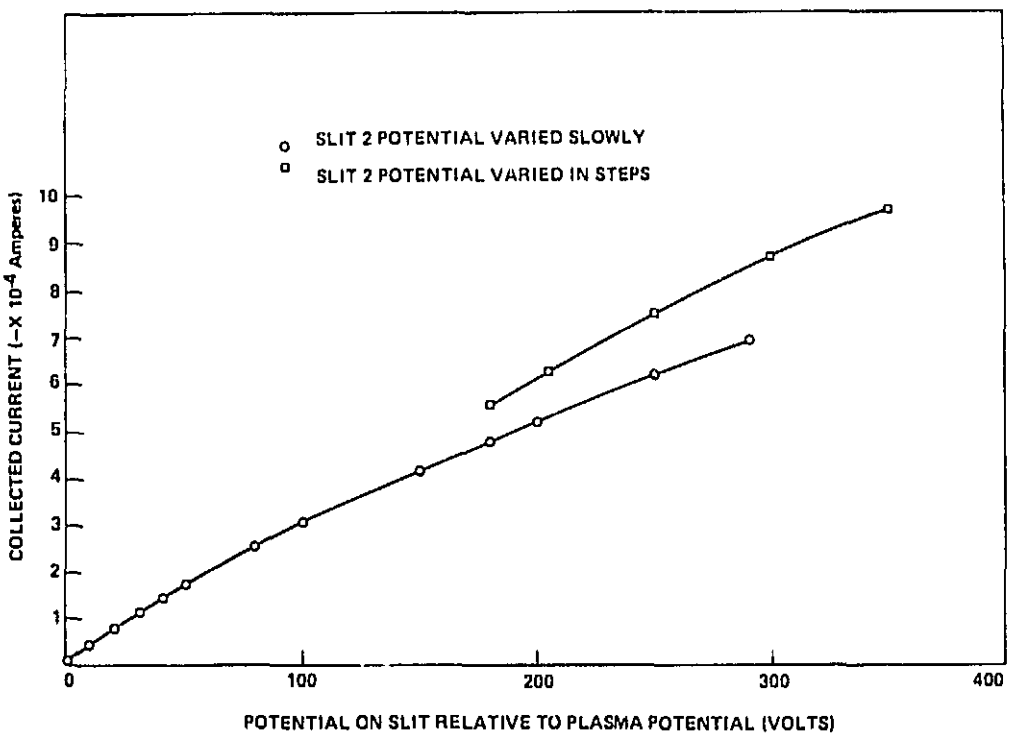

(b)

Figure 17. Current collected by single biased slit.

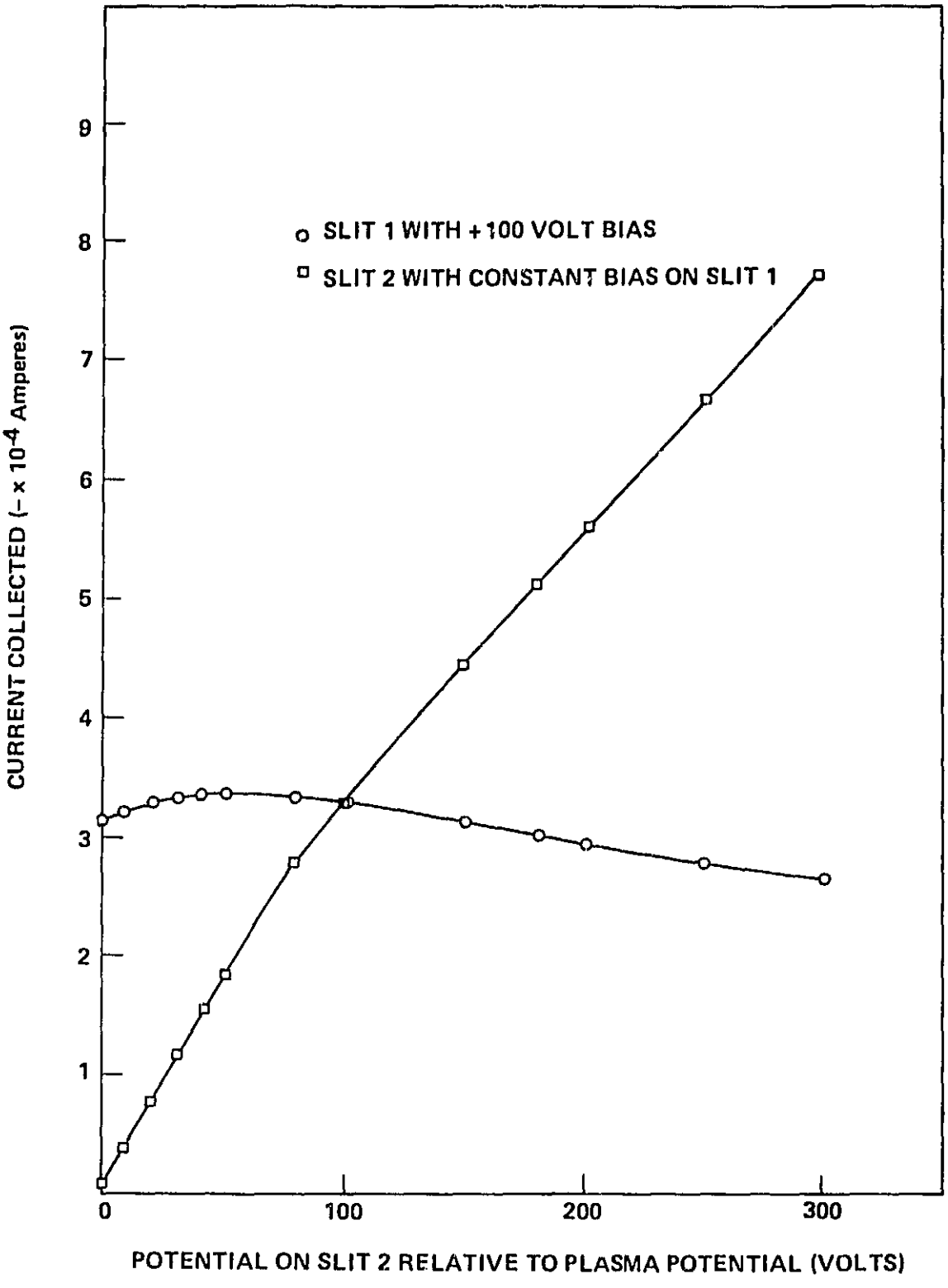

Figure 18. Current for two biased slits: One +100 V and the other varied.

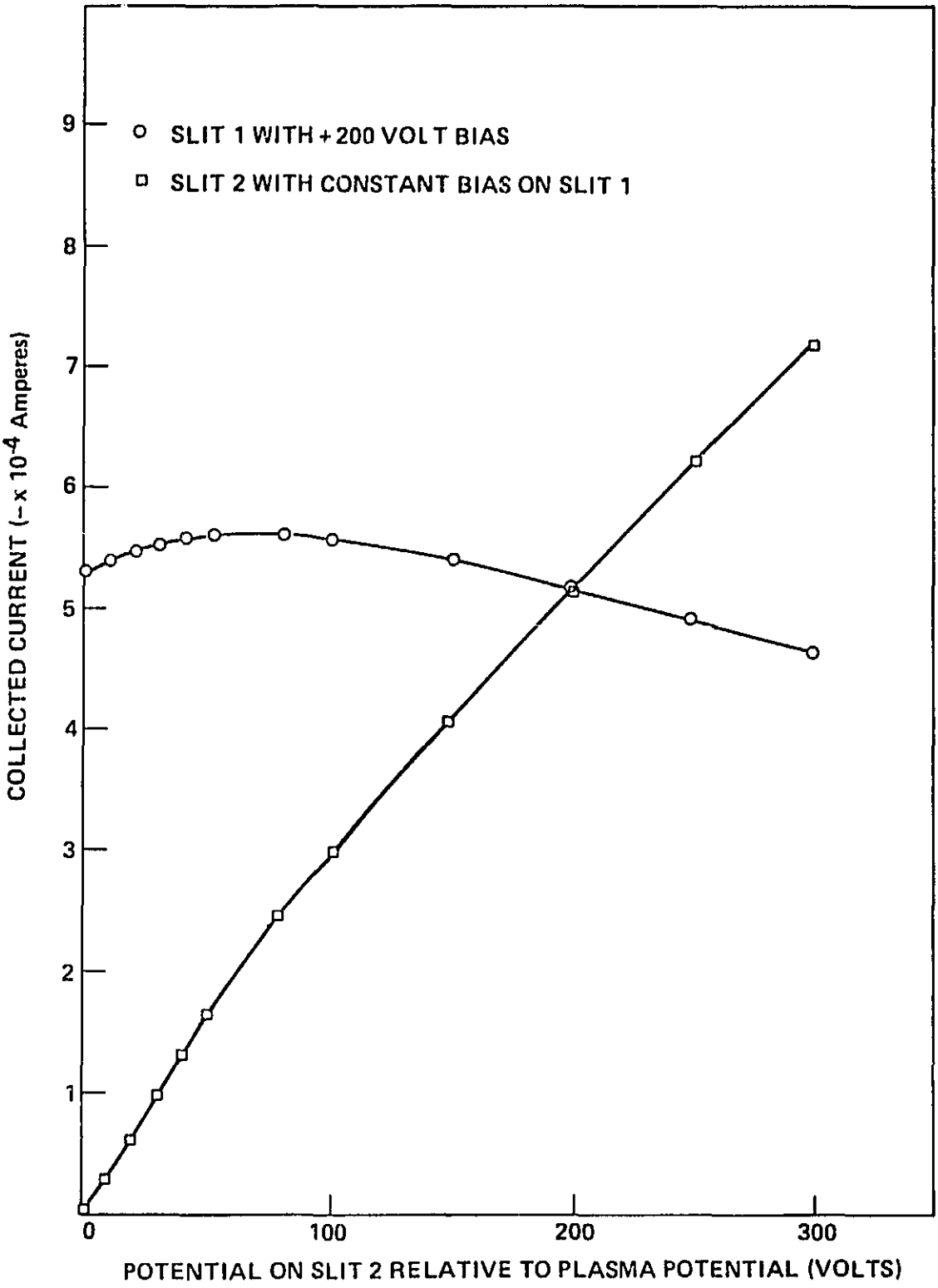

Figure 19. Current for two biased slits: One +200 V and the other varied.

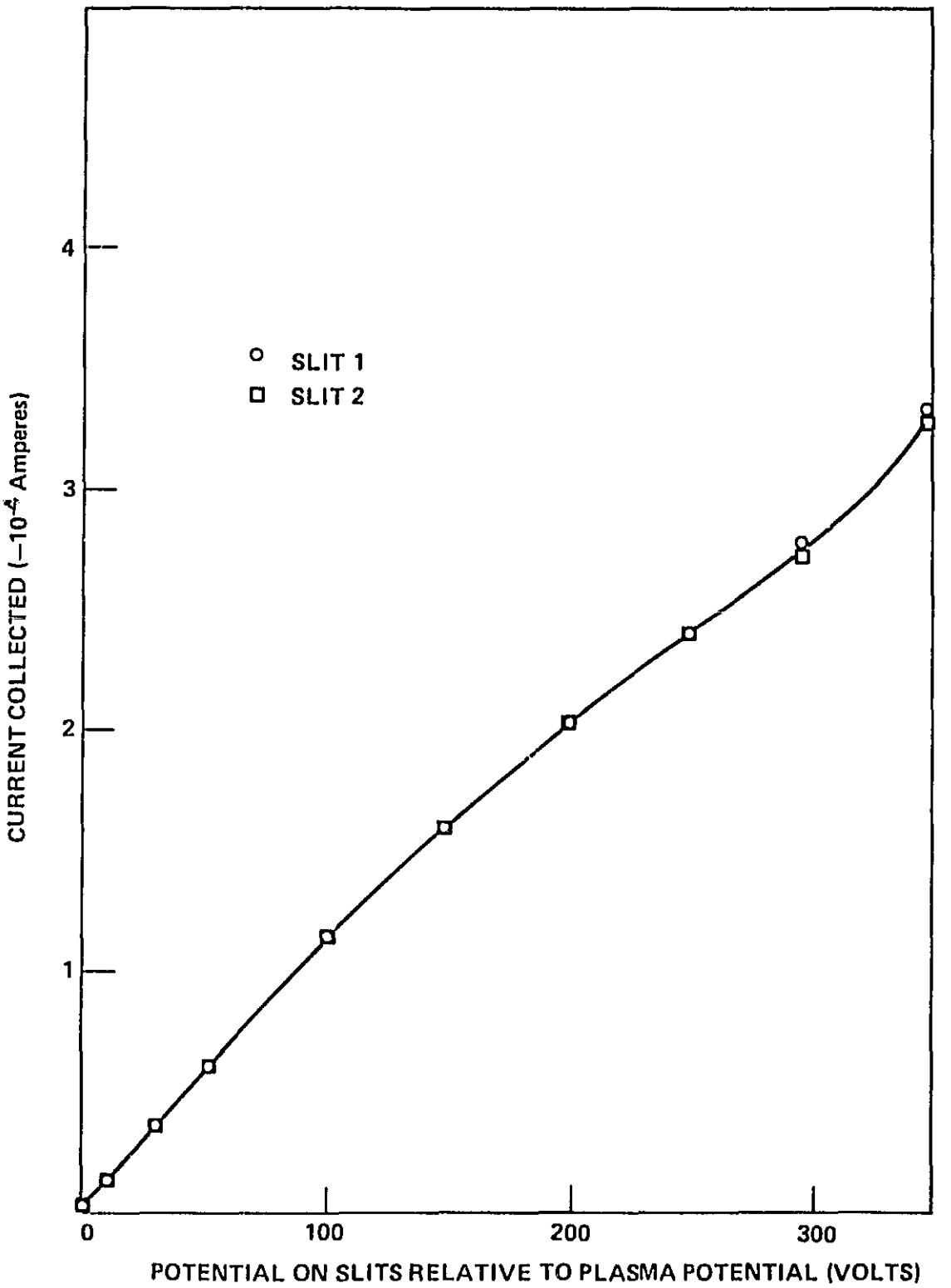

Figure 20. Current collected by single biased slit.

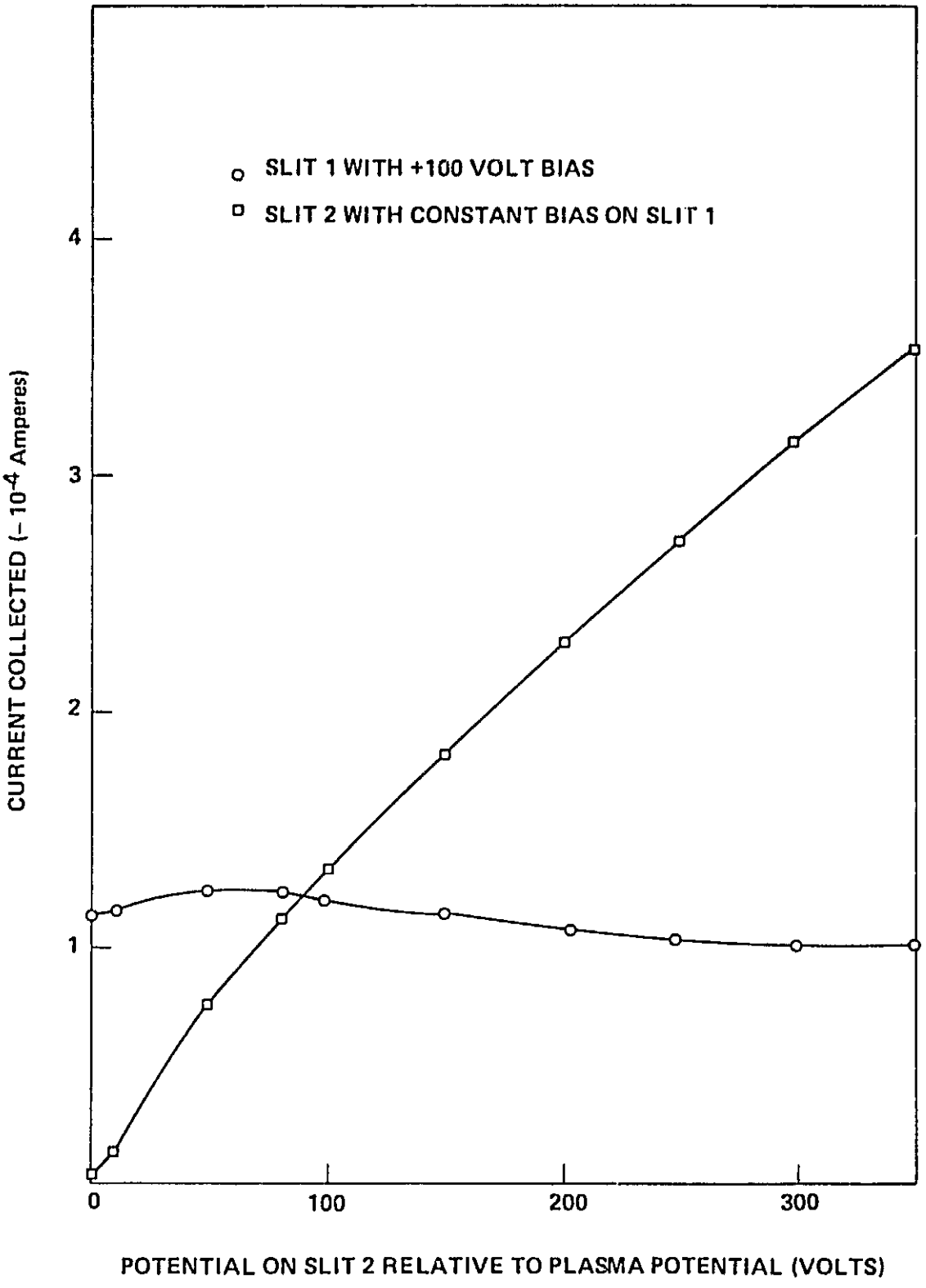

Figure 21. Current for two biased slits: One +100 V and the other varied.

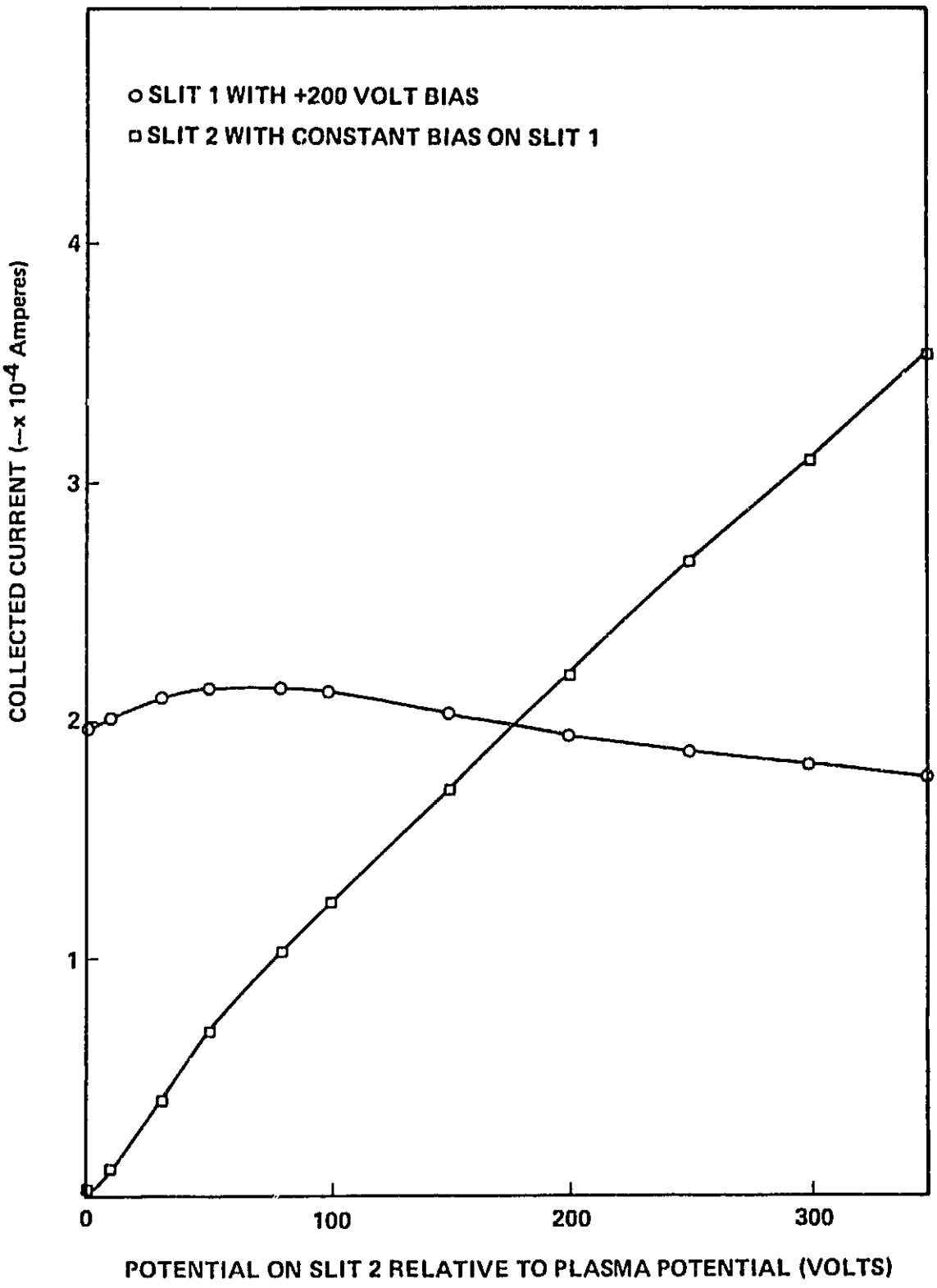

Figure 22. Current for two biased slits: One +200 V and the other varied.

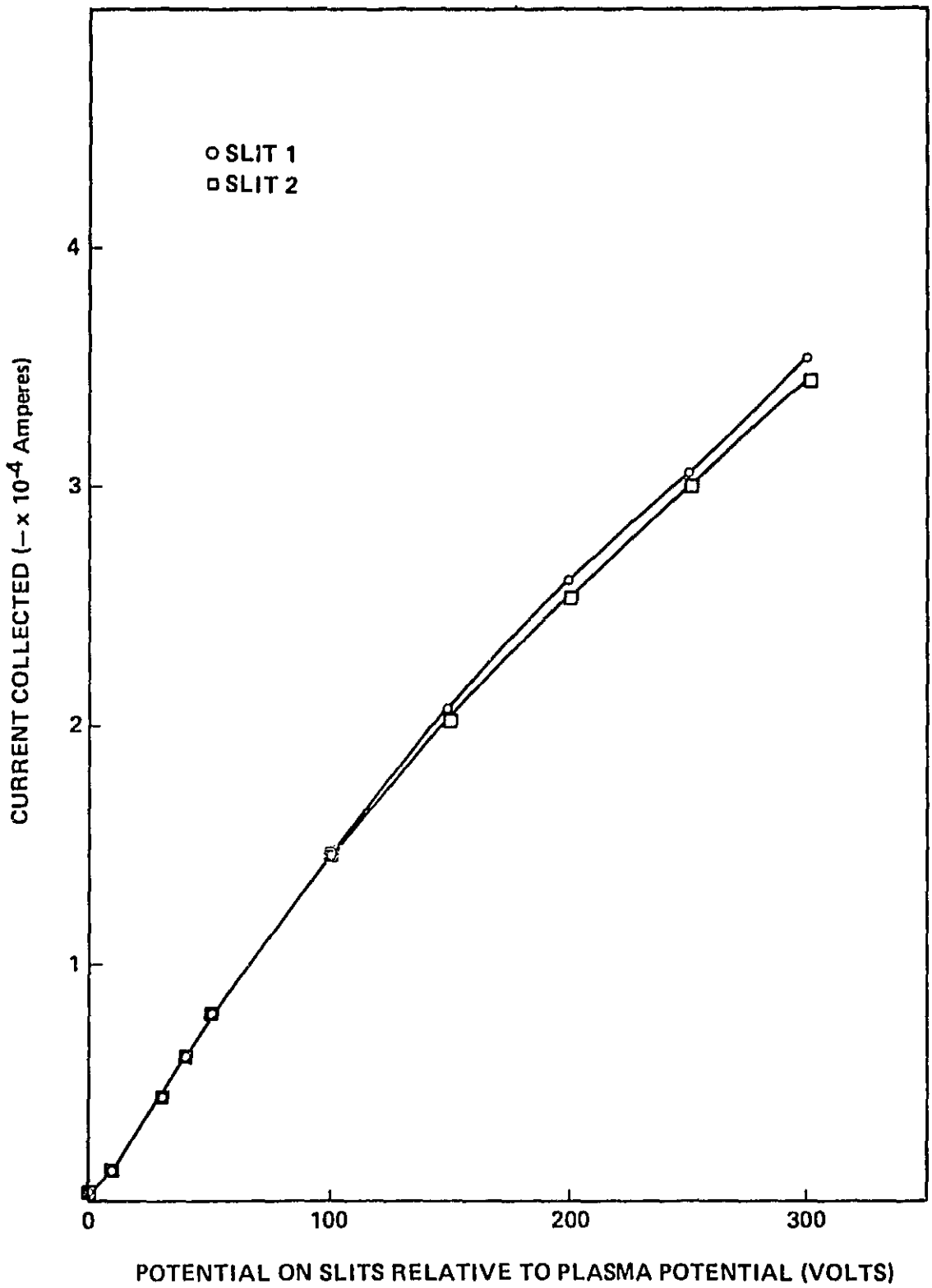

Figure 23. Current collected by single biased slit.

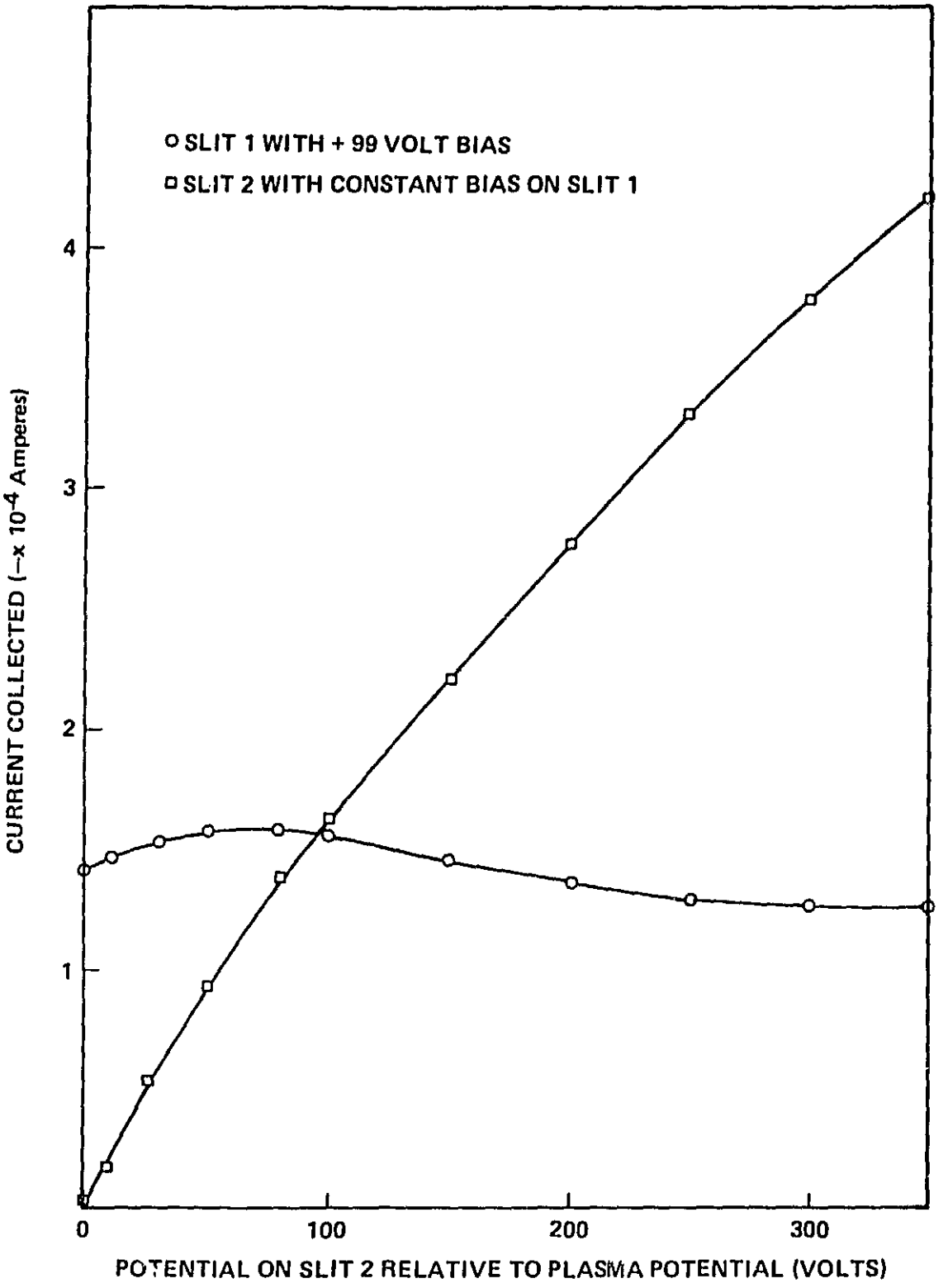

Figure 24. Current for two biased slits: One +99 V and the other varied.

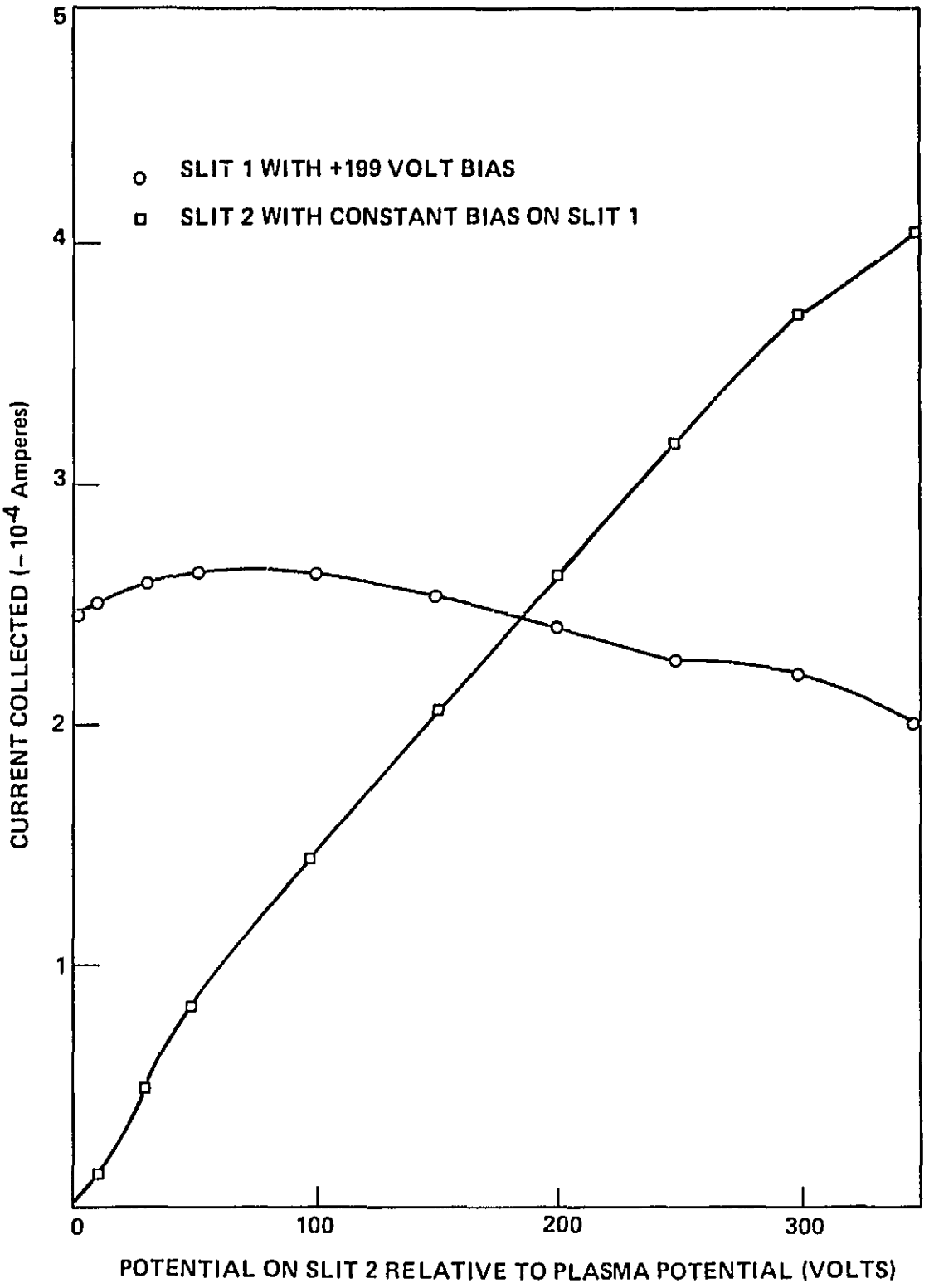

Figure 25. Current for two biased slits: One +199 V and the other varied.

electric field reversal point still becomes distinguishable. This still then becomes a barrier but the electrons entering the sheath are initially drawn to the higher potential. A steeper gradient and/or an increase in potential of both slits relative to the plasma potential will result in even more current collection by the higher potential slit at the expense of the one at lower potential. An examination of the data given in the figures reveals that the current collected by slit 2 at a specified high potential is greater when slit 1 is at +100 V as opposed to +200 V.

For all the cases where the potential on slit 1 was set to +100 V, its collected current did not decrease until the potential on slit 2 was increased to about +100 V. However, for the cases where the potential on slit 1 was set at +200 V and the other varied, the current collected by slit 1 at +200 V began to drop well before slit 2 was brought up to +200 V. A possible explanation for this observation is given. With slit 1 set at a specified potential, the slit 2 potential is increased from zero, at which time there is little or no sheath around it and it cannot contribute current to the slit held at constant potential. As the potential on the slit 2 is increased, the sheath around it begins to grow and merge with the sheath from the slit with constant potential and therefore additional current is only then made available and supplied to slit 1. As the potential is increased on slit 2, the electric field reversal point between them moves toward slit 1 and the current collected by it begins to decrease. For set distances between the slits, the sheaths are larger for the constant +200 V potential relative to the +100 V potential. Therefore, the effect of the movement of the field reversal point is more pronounced for the case of higher potential and therefore the current starts dropping sooner.

It is anticipated that the sheath area for the two slit sheaths coalesced is smaller than the sum of the two sheath areas when they are biased individually. An examination of the currents collected for the slits biased together and independently indicates that the total current collected is nearly the same. A slight trend in the expected direction appears to exist but the data were not conclusive.

The current collected by individual slits is observed to be a linear relationship with potential relative to the plasma. This is consistent with the large pinhole experiments of Gabriel, et al., and Kennerud. In the introduction to this report, it was stated that large increases in current have been reported to occur for positive potentials greater than +100 V. However, this was generally for small defects or pinholes [6]. The larger sizes in this experiment were chosen to ensure sheath expansion at modest potentials.

Some observations were made which warrant discussion but data were not obtained in sufficient detail to include in this report. They will be mentioned here for general interest. Some observations of the sheath for negatively applied potentials were made. Consistent with other experimenter results, the sheath penetration into the plasma was considerably smaller than for a corresponding positive potential bias. Also, some looks at the current collection by the slits were made for stepping of the potential rather than the slow variation. This led to the previously described second collection mode involvement in the current collection. When slit 1 was biased to a set potential, it collected a given amount of current as reported. When the high potential was suddenly applied to slit 2, it collected initially a large amount of current. Correspondingly, the current collected by slit 1 dropped to about one-fourth of the current collected before the potential was applied to slit 2. After a period of a few seconds, both slits stabilized to constant values of current collection with the difference in the current collected by the two slits at the given bias potentials greater than the case where the slit 2 potential was increased slowly.

CONCLUSIONS

The experimental data indicate that a voltage difference between two biased slits in a plasma, where their respective sheaths begin to overlap, leads to an increase in electron current collection by the one with higher positive potential. Even for small potential differences it is noticeable and for differences of several tens of volts per centimeter the effect is significant. The electron collection by the most positive slit increases as the condition where the x-axis electric field reversal point moves toward the slit with lower potential and ultimately disappears or is prominent only deep within the sheath. For given positive biases, the total current collected by both slits when their sheaths have merged is approximately that collected by the slits biased independently.

The semi-empirical formulation for the sheath structure given by Gabriel, et al., may be used to calculate the potential and electric field distribution about biased multiple pinholes or slits. However, it is limited by the fact that experimental parameters must be input and some parameters identified as constants actually vary with position. This restricts the extrapolation to regions where data are not obtained.

The question of what is the solar array power loss due to the collection of charged particles from the plasma is a difficult one to answer because of the complexity of the current collection and how it affects array performance. The role played by charged particle transport by voltage gradients on the array is in itself very complex but some general conclusions as to its importance may be stated. If the potential difference between solar cells in an array can be maintained such that everywhere strong gradients do not exist and the sheath maintains a "bumpy" potential distribution (electric field reversal on x axis) then the effects of such gradients will probably have a small effect on array performance. If this is not the case, then these gradients may significantly add to the solar array power loss. As already stated, other solar array design considerations may mean that large voltages and gradients will exist on the surface of a solar array. The results of the study reported herein indicate that consideration should be given to the effects these surface potential variations will have on solar array performance.

REFERENCES

1. Stevens, N. J.: Interactions Between Spacecraft and the Charged Particle Environment. Spacecraft Charging Technology-1978, NASA CP-2071, 1978.

2. Stevens, N. J.: Investigation of High Voltage Spacecraft System Interactions with Plasma Environments. AIAA Paper No. 78-672, 1978.

3. Stevens, N. J.: Large Space System-Charged Particle Environment Interaction Technology. NASA TM-79156, also AIAA Paper No. 79-0913, May 1979.

4. Grier, N. T.: Experimental Results on Plasma Interactions with Large Surfaces at High Voltage. NASA TM-81423, 1980.

5. Suh, P. K., and Stauber, M. C.: Photoelectron Drift and Multiplication Due to Surface Potential Gradient; Application to Solar Power Arrays. AIAA Paper No. 80-0044, January 1980.

6. Kennerud, K. L.: High Voltage Array Experiments. NASA CR-121280, 1974.

7. Chaky, R. C., Nonhast, J. H., and Armstrong, T. P.: Numerical Simulation of Plasma-Insulator Interactions in Space. Part II: Dielectric Effects. Spacecraft Charging Technology-1980. NASA CP-2182, 1980.

8. Gabriel, S. G., Garner, C. E., and Kitamura, S.: Experimental Measurements of Plasma Sheath Around Pinhole Defects in a Simulated High Voltage Solar Array. AIAA Paper No. 83-0311, 1983.

9. Kaufman, H. R., and Robinson, R. S.: Inert Gas Thrusters. NASA CR-165332, December 1980.

10. Stillwell, R. P., Robinson, R. S., Kaufman, H. R., and Capp, R. K.: Experimental Investigation of an Argon Hollow Cathode. AIAA Paper No. 82-1890, November 1982.

11. Aston, G. and Wilbur, P. J.: Ion Extraction from a Plasma. J. Appl. Phys., Vol. 52, No. 4, April 1981.

12. Chen, F. F.: Electric Probes. Plasma Diagnostic Techniques. Edited by R. H. Huddlestone and S. L. Leonard, Academic Press, New York, 1965.

APPROVAL

SURFACE VOLTAGE GRADIENT ROLE IN HIGH VOLTAGE SOLAR ARRAY/PLASMA INTERACTIONS

Center Director's Discretionary Fund Final Report

By M. R. Carruth, Jr.

The information in this report has been reviewed for technical content. Review of any information concerning Department of Defense or nuclear energy activities or programs has been made by the MSFC Security Classification Officer. This report, in its entirety, has been determined to be unclassified.

A. J. DESSLER
Director, Space Science Laboratory

☆U.S. GOVERNMENT PRINTING OFFICE 1985—544-048/20006